CERN-ACC-NOTE-2024-0021
November 8, 2024
marten.koopmans@cern.ch

The Acceptance Box – A Simple Diagnostics Tool for Source Optimization and Transverse Beam Matching

M. Koopmans, J.-B. Lallement, A. M. Lombardi, E. Marchetti, E. Pasino, and E. Sargsyan
CERN, Geneva, Switzerland

Abstract

The measurement of the emittance and Twiss parameters of a low to medium energy ion beam is a time intensive procedure and requires special hardware as well as data acquisition and analysis. Especially for the commissioning and optimization of sources and Low Energy Beam Transport (LEBT) lines for the injection into Radio Frequency Quadrupoles (RFQs) it is however not always necessary to have the full phase space information of the beam. The main question is often just to know how much of the ion beam falls into the transverse RFQ acceptance and can be accelerated. For this purpose, the so-called RFQ acceptance box has been developed at CERN. It reproduces the transverse RFQ acceptance and in combination with a Faraday cup allows for fast methods to optimize the source and the LEBT to match the beam to the RFQ. In this paper the general principle of the acceptance box and how to define its parameters is introduced starting from basic beam dynamics. Examples of acceptance boxes produced for different RFQs at CERN are presented. Finally, the working principle of the acceptance box is validated with simulations and measurements.

Keywords: Acceptance Box, Transverse Phase Advance, Transverse Emittance Diagnostics, Ion Source and LEBT Optimization

Contents

1 Introduction

The knowledge of the transverse beam parameters, beam sizes, Twiss parameters and especially emittances inside accelerators is crucial for the commissioning as well as operation and optimization of different accelerator structures. For storage rings as well as for Linacs it is important to ensure stable conditions and mitigate losses. An overview about the transverse emittance and measurement techniques to obtain it is given in Ref. [1]. The most popular methods for ion beams are for example: The combination of a movable slit plus a downstream wire grid, the combination of two movable slits at different positions plus a Faraday cup, a profile measurement in combination with a quadrupole scan, a pepper pot, or the measurement of the beam profile at three different positions. All methods, in addition, require a dedicated analysis to obtain the emittance from the measurement data.

For this note we will focus on the low and medium beam energies between some tens of keV up to a few MeV inside ion Linacs. Especially the injection of the ion beam into a Radio Frequency Quadrupole (RFQ), which bunches and accelerates the beam to high energies in the range of hundreds of keV to some MeV, is a critical step. The so-called acceptance of an RFQ in the transverse planes is defined by the maximum continuous transverse emittance area effectively accelerated through the structure at the start of the RFQ, the RFQ Matching Plane (MP). To achieve proper matching and focusing of the beam into the transverse RFQ acceptance usually a dedicated Low Energy Beam Transport (LEBT) line is designed. Thus, it is crucial to know transverse beam parameters, its emittance and Twiss parameters, at the RFQ MP for the design and commissioning of the source and the LEBT. A very effective procedure used to obtain emittance and Twiss parameter information of the beam at the MP of the Linac4 RFQ based on slit grid emittance measurements has been described in [2]. It has been extensively used to estimate beam current falling into the RFQ acceptance and the matching conditions [3].

The measurement of the emittance and Twiss parameters is time intensive and requires special hardware, data acquisition, and data analysis. However, for source optimization and LEBT commissioning it is in many cases sufficient just to know the fraction of the beam which falls into the RFQ acceptance. Therefore, a more rapid method has been developed and put in place in parallel. This method is based on mimicking the transverse RFQ acceptance by a series of transverse aperture limitations, representing the so-called acceptance box, and collecting the ions which fall in the transverse RFQ acceptance by measuring the current with a Faraday cup behind the acceptance box. This method, besides being faster, is more suitable for an automatic optimization of source and LEBT parameters [3].

The RFQ acceptance box consists of intercepting plates with squared aperture restrictions. The aperture sizes and their relative distances are chosen such that only the particles within the transverse RFQ acceptance can pass through all four aperture restrictions. Extensive calculations under different regimes of space charge distribution and intensity have been performed to validate this device. However, the use case of the acceptance box is not limited to only imitate transverse RFQ acceptances. The principle is in general valid and can be used to measure which part of a beam falls into a transverse emittance with respect to a reference plane. While the principle will be explained generally, the examples and applications in this paper will concentrate on the application to simulate RFQ acceptances.

First, the general principle of the acceptance box and how to define its parameters is introduced and outlined in Section 2. Three examples of acceptance boxes designed for RFQs at CERN are given in Section 3. Finally, simulations to validate the working principle of the acceptance box are performed and comparison of measurements are presented for the Linac4 RFQ in Section 4.

2 Acceptance Box

This section introduces the general working principle of the acceptance box, a device that can select the portion of a particle beam inside a given transverse phase space area with multiple subsequent aperture limitations. For the explanation we will consider a one-dimensional, uniform, converging beam and use the position of the beam waist as reference plane. First, the transverse phase advance in a drift is introduced in Section 2.1, then the connection of the phase advance to confining the transverse phase space area is demonstrated in Section 2.2, and examples how to define an acceptance box are given in Section 2.3. Finally, the extension to two dimensions and the limitations of the method are discussed in Section 2.4.

2.1 Transverse Phase Advance

The acceptance box principle is based on linear beam dynamics considerations in a drift space in absence of space charge effects. The transverse phase advance ψ between two longitudinal positions L_0 and L along the z-coordinate is defined as the integral of the inverse of the β-function [4]

$$\psi(L_0 \to L) = \int_{L_0}^{L} \frac{\mathrm{d}z}{\beta(z)}, \tag{1}$$

where β is one of the Twiss parameters α, β and γ used to describe a beam phase space ellipse. In a drift the β-function can be calculated using the corresponding matrix transformation for the Twiss parameters [4]

$$\begin{pmatrix} \beta(L) \\ \alpha(L) \\ \gamma(L) \end{pmatrix} = \begin{pmatrix} 1 & -2\Delta L & \Delta L^2 \\ 0 & 1 & -\Delta L \\ 0 & 0 & 1 \end{pmatrix} \begin{pmatrix} \beta_0 \\ \alpha_0 \\ \gamma_0 \end{pmatrix}, \tag{2}$$

where α_0, β_0 and γ_0 are the Twiss parameters at the initial position L_0 and $\Delta L = L - L_0$. Thus, the β-function is given by

$$\beta(L) = \beta_0 - 2\alpha_0 \Delta L + \gamma_0 \Delta L^2. \tag{3}$$

Assuming a converging beam, we will set the reference position of the drift to the beam waist for simplicity. Considering $\beta\gamma - \alpha^2 = 1$ the Twiss parameters at the beam waist are by definition

$$\begin{aligned} \alpha_0 &= 0, \\ \gamma_0 &= 1/\beta_0. \end{aligned}$$

So by setting $L_0 = 0$ at the waist, the β-function is completely defined by β_0 at the waist

$$\beta(L) = \beta_0 + \frac{L^2}{\beta_0} = \frac{\beta_0^2 + L^2}{\beta_0}. \tag{4}$$

Inserting this into the transverse phase advance relation Eq. (1), one can solve the integral for a drift space after the waist

$$\psi(L) = \int_0^L \left(\frac{\beta_0}{\beta_0^2 + z^2} \right) \mathrm{d}z = \int_0^L \frac{\mathrm{d}z/\beta_0}{1 + (z/\beta_0)^2} = \arctan\left(\frac{L}{\beta_0} \right). \tag{5}$$

For $L \to \infty$ the phase advance $\psi \to \pi/2$, thus considering the symmetry around the waist, the maximum total phase advance in a drift is π or 180° for any $\beta_0 > 0$ [4]. Making use of the symmetry around the waist, the relative phase advance with respect to the waist is used in the following. The β-function and the corresponding transverse phase advance relative to the waist are shown exemplarily for $\beta_0 = 1\,\mathrm{m/rad}$ in a drift space around the waist in Fig. 1. The β-function describes a parabola and the relative transverse phase advance approaches $\pm 90^\circ$ for large distances from the waist, as discussed above.

2.2 Transverse Emittance Evolution

To demonstrate the connection between the transverse beam size and the transverse phase advance in a drift space we will use a uniform example beam with the waist as reference plane. The beam is shown in Fig. 2 with a geometric RMS emittance $\varepsilon_{\mathrm{RMS}} = 0.25\,\mathrm{mm\,mrad}$, maximal extensions of $x_{0,\mathrm{max}} = 1\,\mathrm{mm}$, $x'_{0,\mathrm{max}} = 1\,\mathrm{mrad}$, and $\beta_0 = 1\,\mathrm{m/rad}$. The resulting transverse phase space in a drift can be calculated using the matrix transformation for a single or multiple particles

$$\begin{pmatrix} x \\ x' \end{pmatrix} = \begin{pmatrix} 1 & L \\ 0 & 1 \end{pmatrix} \begin{pmatrix} x_0 \\ x'_0 \end{pmatrix}, \tag{6}$$

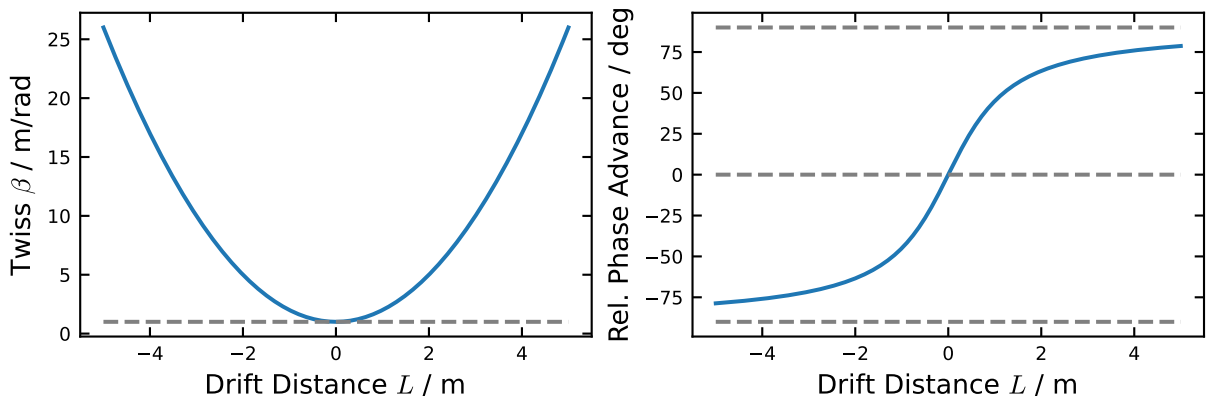

Figure 1: Evolution of the Twiss β-function corresponding to Eq. (4) (left) and phase advance relative to the waist corresponding to Eq. (5) (right) in a drift space.

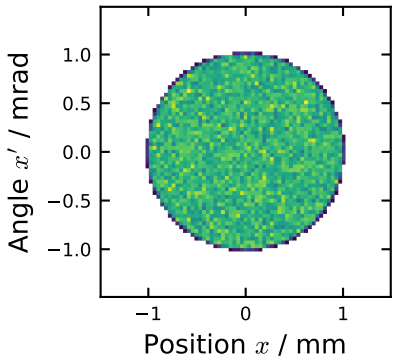

Figure 2: Uniform one-dimensional example beam at the waist in x-x'-phase space with a geometric RMS emittance of $0.25\,\mathrm{mm\,mrad}$ used for the introduction and demonstration of the acceptance box in this section.

where L is the drift distance, x_0 the initial position, and x'_0 the initial angle, which does not change in a drift. On the other hand, we already know how to calculate the phase advance of the beam in a drift of a certain distance from the waist from the previous section. Solving Eq. (5) for the position yields

$$L = \beta_0 \tan\psi. \tag{7}$$

The drift from the waist of the demonstration beam in Fig. 2 to the positions $L_i = 0.577\,\mathrm{m}$, $1\,\mathrm{m}$, $1.732\,\mathrm{m}$ corresponding to phase advances of $\psi_i = 30°, 45°, 60°$ from the waist is illustrated in Fig. 3. It shows the transverse phase ellipses at the respective drift positions and how it deforms and that the beam gets broader for larger drift distances from the waist. In addition, the respective phase advances are indicated in the transverse phase advance as function of the drift distance relative to the waist and the particles, which are at the corresponding "angle" in the transverse phase space, are highlighted in the transverse phase spaces of the beam at the waist. These particles are also highlighted in the transverse phase space plots at the respective drift positions. Looking at these particles at the drifted positions it becomes clear that these are exactly the particles at the edge of the beam with the maximum x positions after the drift. Thus, the outer particles in x after a certain drift distance correspond to an initial "angle" in the transverse phase space at the waist equal to the relative phase advance from the waist. The same is true for the minimum x position and as well for drifts in negative z direction.

For this simple example beam at the waist, the maximum beam position $x_{\max}$ can be described directly with the β-function given in Eq. (4). Utilizing the relation $\varepsilon\beta = \langle x^2 \rangle$, where ε is the emittance, and that the emittance stays constant in a drift, one can derive

$$\frac{x_{\max}(L)}{x_{0,\max}} = \sqrt{\frac{\beta(L)}{\beta_0}} \Rightarrow x_{\max}(L) = x_{0,\max}\sqrt{\frac{\beta_0^2 + L^2}{\beta_0^2}}. \tag{8}$$

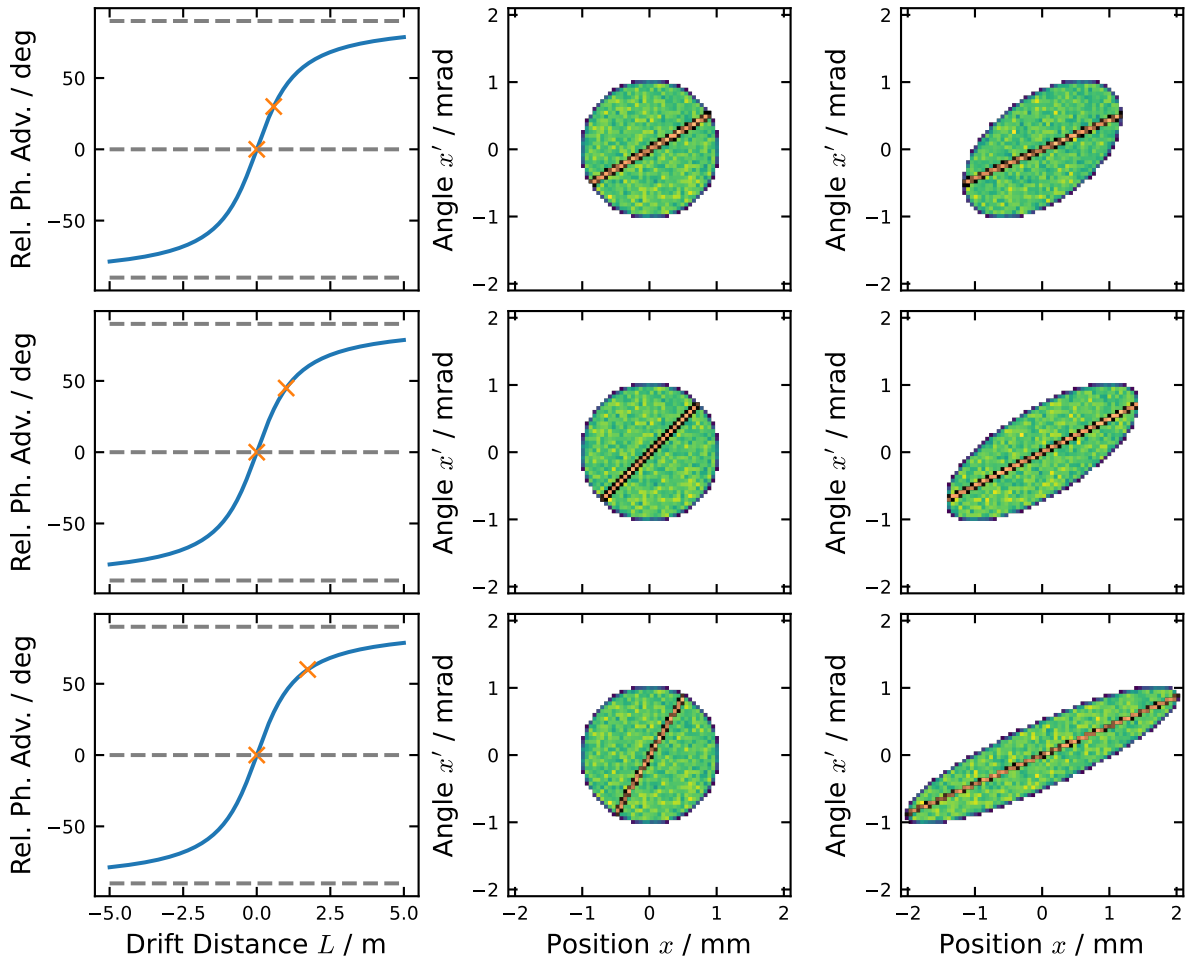

Figure 3: Illustration how the transverse phase space of the demonstration beam from Fig. 2 evolves in a drift in connection to the transverse phase advance. It shows the transverse phase advance relative to the waist as function of the drift distance L (left) and the transverse phase space of the beam at the waist (middle) as well as after drift of $L_i = 0.577\,\mathrm{m}$, $1\,\mathrm{m}$, $1.732\,\mathrm{m}$ (right) corresponding to a phase advance of $\psi_i = 30°$, $45°$, $60°$ from the waist (top to bottom). The positions where these phase advances are reached are marked in the relative phase advance plot. In addition, the particles which are at the corresponding "angle" in the transverse phase space at the waist are highlighted in the transverse phase space plots at both positions.

The maximum beam size according to Eq. (8) is plotted in Fig. 4 as function of the drift distance from the waist. It resembles the envelope of a beam with the typical waist, while approaching linear expansion further away from the waist.

2.3 Defining the Acceptance Box Parameters

Making use of this basic relation between the transverse phase advance and the transverse beam size, one can confine a region in the transverse phase space. Ideally a continuous aperture limitation following the maximum beam size at each position as shown in Fig. 4 would exactly accept all particles within the boundaries of the demonstration beam at the waist reference position. However, such a funnel-like beam pipe is costly and inflexible. It will be demonstrated in the following that a sufficient confinement of the transverse phase space can already be achieved with a few apertures at certain positions. To define the parameters, first the number of apertures is chosen. Considering again the illustration of the drift in the transverse phase space in Fig. 3 it is evident that one wants to put the apertures such that they are maximally apart in terms of transverse phase advance to evenly confine the phase space region with a regular shape of equal "angles".

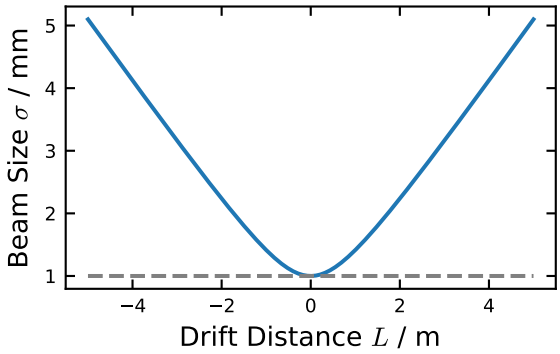

Figure 4: Maximum or $100\,\%$ beam size of the demonstration beam shown in Fig. 2 in a drift as a function of the drift distance from the waist corresponding to Eq. (8).

The principle is demonstrated alongside an example, defining the acceptance box parameters for the uniform beam from Fig. 2 at the waist as reference plane. We will start with an example for a four-aperture setup in the symmetric configuration, which is also the most compact solution (see also the discussion of asymmetric configurations below).

The first step is to determine the aperture positions with respect to the reference position. In the case of four apertures a transverse phase advance of $45°$ is wanted between each neighboring apertures. Thus, in the compact symmetric configuration, the apertures are placed at $\psi_i = \pm 22.5°$ and $\pm 67.5°$ from the waist. The aperture positions $L_i = \pm 0.4141\,\mathrm{m}$ and $\pm 2.4142\,\mathrm{m}$ are then calculated using Eq. (7). In a second step the aperture widths d_i are determined. From the obtained positions the beam sizes at these positions are calculated with Eq. (8) and one obtains $d = 1.08\,\mathrm{mm}$ for the inner and $d = 2.61\,\mathrm{mm}$ for the outer aperture widths. The procedure to determine the aperture positions and widths is shown in Fig. 5 together with the transverse phase advance relative to the waist and the maximum transverse beam size, respectively.

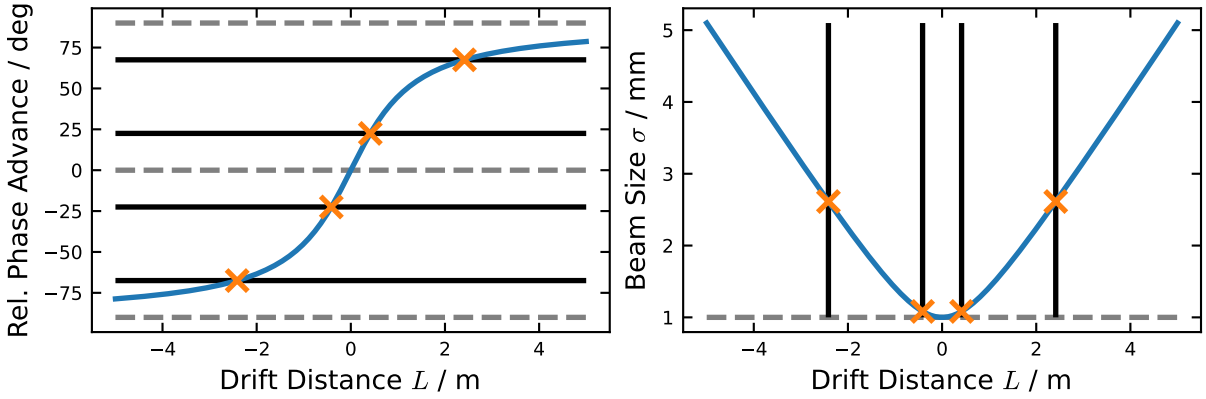

Figure 5: Illustration how the aperture properties of the acceptance box for the demonstration beam from Fig. 2 are determined in the case of four apertures. First, the aperture positions defined by where the relative phase advances $\psi_i = \pm 22.5°, \pm 67.5°$ from the waist are reached (left). Next, the aperture widths are obtained by the maximum beam size at these positions (right).

An illustration of the limitation of a large uniform beam in the transverse phase space with the acceptance box for the demonstration beam defined above is shown in Fig. 6. For each aperture the cut in the transverse phase space is subsequently applied in the direction of the beam drift. The transverse phase space is shown with these cuts at the position of the respective aperture and at the waist position of the reference beam, which is the reference plane of the demonstration beam at the waist for which the acceptance box is designed. It is apparent that the phase space resulting from the four cuts at the different positions in x is a regular octagon at the reference beam position in the x-x'-phase space.

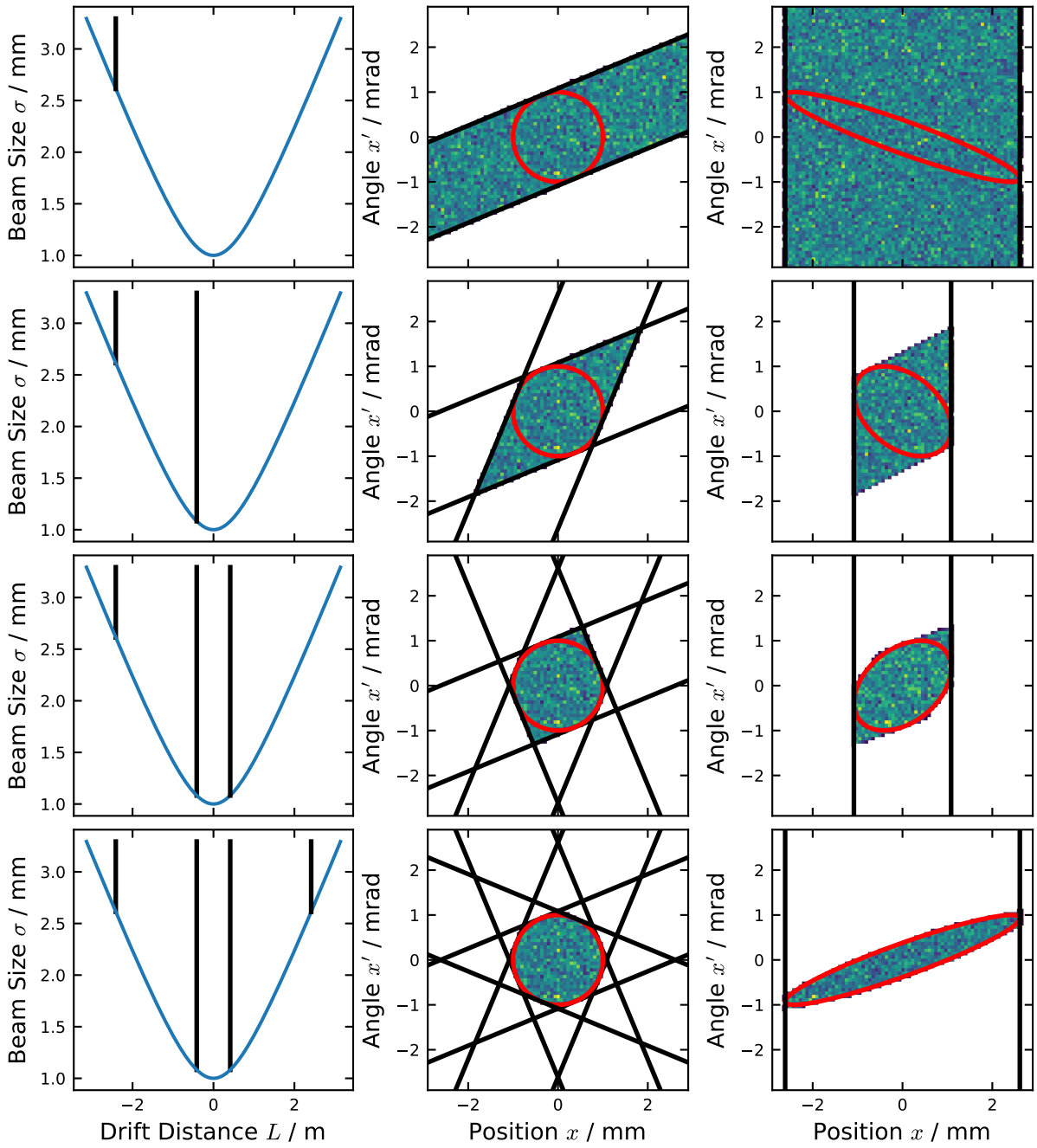

Figure 6: Illustration how the acceptance box determined for the demonstration beam in Fig. 5 confines a large uniform beam in the x-x'-phase space. The aperture cuts in the transverse phase space are applied consecutively in direction of the drift (top to bottom) and are shown together with the maximum beam size from Fig. 4 (left). The corresponding cuts in the x-x'-phase space at the waist as reference plane for the example beam (middle) and at the slit position (right) and are depicted and compared to the edge of the demonstration beam (red ellipse).

In comparison to the ellipse representing the edge of the uniform beam the accepted phase space region is a bit larger since the cuts only tangentially enclose the ellipse. To compensate this effect, it is possible to compromise and cut slightly into the ellipse, so that the total enclosed area would be the same.

While it will become apparent that the configuration discussed above is the most convenient, it is not necessary to place the apertures symmetrically around the waist. The position of all apertures can be shifted simultaneously in phase advance, in principle almost up to $22.5°$, so that there are always two apertures on each side of the waist. However, the closer one aperture gets to the waist, the less compact is the acceptance box. Since the transverse phase advance increases less with further distance, the outer aperture on the other side has to be placed even further away from the waist. An example is given placing

the aperture with a phase shift of $10°$, so at $\psi_i = -57.5°, -12.5°, 32.5°, 77.5°$ relative to the waist. As above the aperture position and widths are defined, which is shown in Fig. 7.

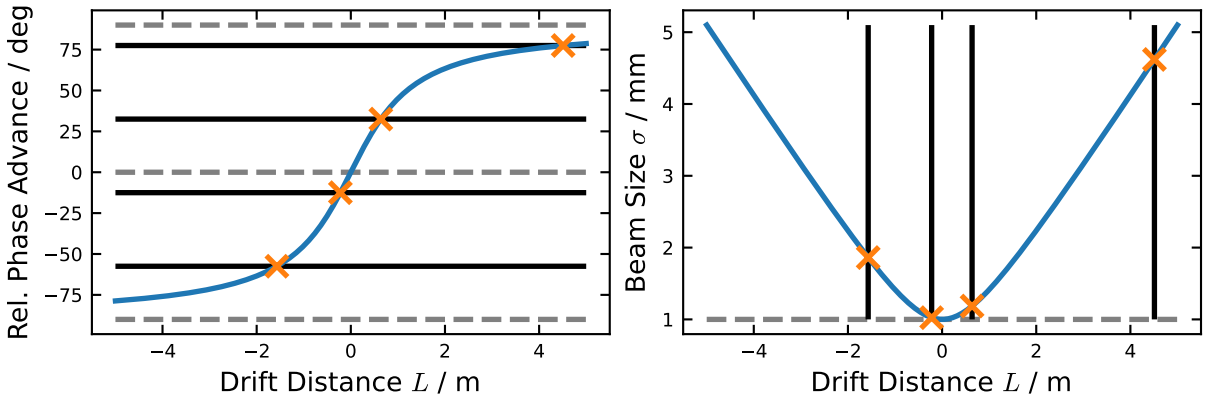

Figure 7: Illustration of the determination of the acceptance box aperture properties for the demonstration beam using four apertures as in Fig. 5, but for a non-symmetric case with phase advances by shifted by $10°$. The aperture positions for the resulting phase advances $\psi_i = -57.5°, -12.5°, 32.5°, 77.5°$ relative to the waist are defined (left) and the aperture widths are obtained at these positions (right).

In comparison to the symmetric case, the distance from the first to the last aperture position, so the total length of the acceptance box, increases from about $5\,\mathrm{m}$ to $6\,\mathrm{m}$ in this example. Therefore, the more compact symmetric configuration is preferred in reality. In addition, the machining is easier if only two sets of aperture widths and two different distances are needed. However, the non-symmetric case might be sensible, if e. g. there is only limited transverse phase advance before waist and the focusing cannot be changed. The comparison of the resulting enclosed transverse phase space at the reference waist position for the symmetric and the shifted acceptance box is shown in Fig. 8. The enclosed areas are identical, but the octagon is rotated exactly by the $10°$ the acceptance box is shifted.

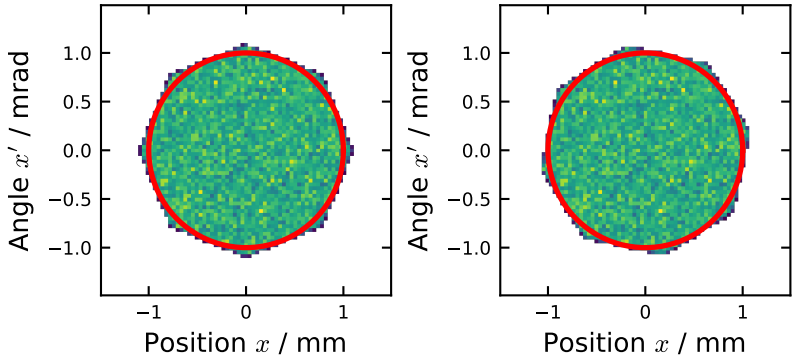

Figure 8: Comparison of the resulting confined transverse phase spaces in x-x'-phase space at the reference waist position using an acceptance box with four apertures in the symmetric configuration as determined in Fig. 5 (left) and in the shifted configuration as in Fig. 7 (right). In addition, the edge of the demonstration beam, for which the acceptance box is designed, is indicated by the red ellipse.

Finally, the effect of the number of apertures is discussed. As mentioned above the more apertures are placed, the more the acceptance box approaches the ideal case of a continuous beam pipe, exactly enclosing the wanted ellipse. This effect is illustrated using two to four apertures for the acceptance box of the example beam. The placement of the slits at the respective positions according to the transverse phase advance around the waist and the enclosed transverse phase space at the reference waist position is shown in Fig. 9. Already with four apertures the ellipse is described quite accurately, with the enclosed area being only about $5\,\%$ larger. As discussed above this can be compensated by cutting a bit into the beam region resulting in the same total area.

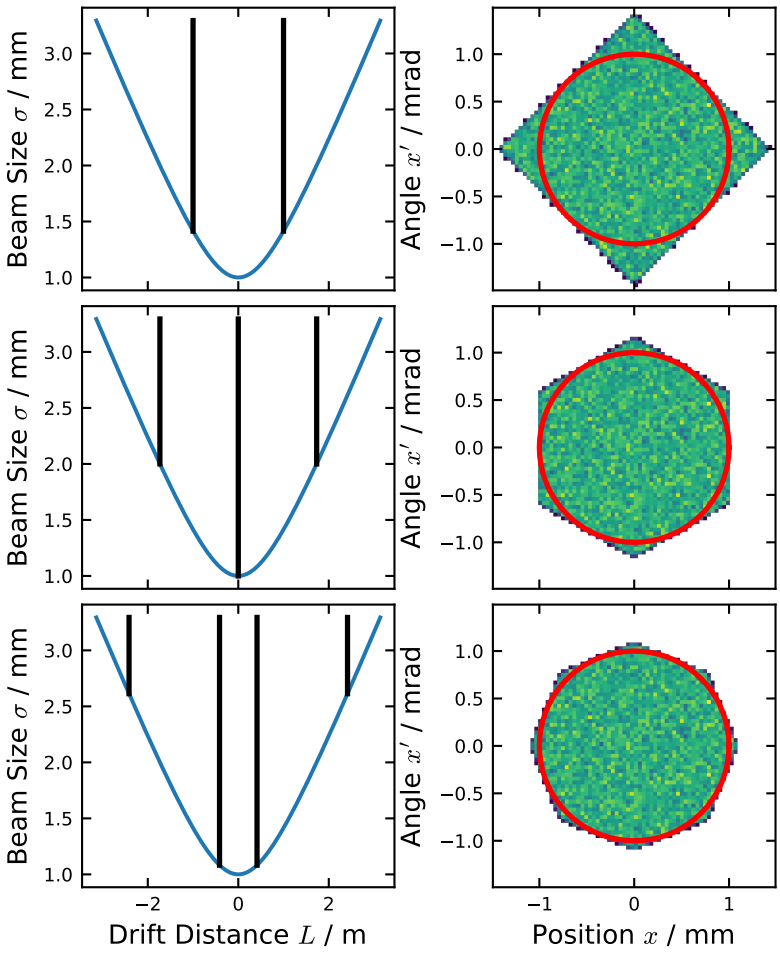

Figure 9: Comparison of acceptance boxes with two, three and four apertures for the demonstration beam (top to bottom). The aperture configurations are shown together with the maximum beam size from Fig. 4 (left) and the resulting confined beam in the x-x'-phase space at the reference waist position (right) are depicted and compared to the edge of the demonstration beam (red ellipse).

2.4 Extension to 2D and Limitations

Until now we only discussed the principle and design of the acceptance box in one transverse dimension. In reality one is, however, usually interested in both transverse dimensions. For the extension to two dimension the acceptance box can in principle be designed independently for each dimension, if x and y are decoupled, but this is not very practical. In general, there are the following options for a two-dimensional acceptance box with four apertures in each dimension:

- Eight 1D apertures. The four aperture positions and widths are defined and placed independently for each dimension.
- Four 2D apertures. If the beam is rotationally symmetric and the four apertures for each dimension would be placed at the same positions, a 2D aperture with identical aperture widths in both dimensions can be used.
- Seven apertures, with six 1D apertures and one 2D aperture, to save one aperture compared to the first case. One can make use of the possibility of shifting the phase of the acceptance box in one dimension and align them at one position. The rest of the 1D apertures are then placed accordingly.

For the general use case as diagnostics for a beam coming out of a source or LEBT, the beam is expected to be close to rotationally symmetric. Therefore, normally an acceptance box with four 2D apertures is used. Another option for non-symmetric beam in other cases is to symmetrize the beam before the acceptance box, to still only require four apertures. Assuming no correlation in the transverse plane the

2D apertures have a squared or more general a rectangular shape. Alternatively, one can use round (or more general elliptical) apertures to only accept a fully correlated beam in the transverse plane.

Due to being a very basic tool the acceptance box has some limitations. It can only ever confirm the transmission of a beam through a single defined transverse phase space region. Therefore, the shape of the transverse acceptance area needs to be reasonably similar to an ellipse. For the result to be useful the beam has to go through a waist and significant drift space before the waist or strong focusing is required for sufficient transverse phase advance. An in principle free parameter is the longitudinal position of the complete acceptance box, moving all four apertures simultaneously. However, this is only applicable, if it is possible to change the position of the reference beam within the setup for the actual experiment. E. g., moving an acceptance box for an RFQ, means that also the RFQ has to be moved, as the acceptance box is designed with respect to the RFQ MP. In addition, the LEBT settings need to be adapted to match the beam has at the new MP position, which can only be done to a certain extend.

Two other limitations of an acceptance box are that it cannot account for possible correlations in the 6D phase space and for space charge. Since the aperture cuts are applied in real space no distinction of other beam parameters and correlations apart from the x-y-plane can be made. In addition, any correlation to the longitudinal phase-space or longitudinal acceptance itself are not considered, since the acceptance box does not discriminate longitudinally. These correlations are especially present considering the 6D acceptance of an RFQ. This can be analyzed in simulations and will be discussed in the next section. A similar issue concerns space charge effects. The acceptance is considered to be a property of the structure, the acceptance box is thus designed assuming zero beam current using linear beam dynamics as explained above.

3 Acceptance Box Examples

In this section we will present three real life examples of acceptance boxes that are in use at CERN. All of them are designed to imitate the acceptance of RFQs, which is our most common use case. However, the transverse acceptance of an RFQ is not a straight-forward parameter. The separate 2D acceptances in both transverse dimensions depend on the longitudinal phase and beam energy and in addition may correlate with each other as well [5]. Thus, the transmission of a beam through an RFQ always depends on its distribution and correlation in the 6D phase space. Therefore, there is no single definite acceptance box design and the parameters may vary within a certain range.

In the following we will give three examples, which can be used as guideline or recipe to find the transverse RFQ acceptance and define the corresponding acceptance box. The first is the acceptance box for the carbon RFQ, which is part of the project for a carbon Linac for hadron therapy in Section 3.1. Next is the acceptance box for the alike RFQs of the ELISA and MACHINA projects in Section 3.2. Finally, the acceptance box for the Linac4 RFQ, which is used at the Linac4 source test stand, is presented in Section 3.3. The design process of the acceptance box for the carbon RFQ will be described in detail. The acceptance of the carbon RFQ is explained, the derivation of the aperture parameters is demonstrated, the acceptance of the RFQ and the acceptance box are compared and discussed. For the other two RFQs the acceptance is discussed and directly the obtained acceptance box parameters are presented. All examples feature an acceptance box with four apertures.

3.1 Carbon RFQ Acceptance Box

The carbon RFQ is the follow-up project the HF-RFQ operating at $750\,\mathrm{MHz}$, which was patented at CERN [6] and is part of a Linac-based proton therapy facility LIGHT [7, 8]. The design of the RFQ has been modified to accelerate ions with $q/m = 1/2$, e. g. carbon $^{12}\mathrm{C}^{6+}$ or helium $^{4}\mathrm{He}^{2+}$ [9, 10] and a full carbon Linac for hadron therapy has been proposed [11]. The RFQ consists of two cavities with a length of $2.5\,\mathrm{m}$ to ensure a stable RF field at its frequency and features a trapezoidal vane geometry. It accelerates the ions from an input energy of $15\,\mathrm{keV}$ to $2.5\,\mathrm{MeV}$ with the first and then to $5\,\mathrm{MeV}$ with the second cavity. More details on the design and parameters of the carbon RFQ can be found in Refs. [9–11]. In the scope of this note only the RFQ acceptance is relevant to demonstrate the design and principle of an acceptance box for an RFQ.

The carbon RFQ acceptance is determined by multi-particle simulations with the tracking code Travel [12]. The beam dynamics simulations are performed using an electric field map of the RFQ obtained with Comsol [13]. To determine the acceptance of the carbon RFQ a large uniform uncorrelated beam in 6D space is used. This beam is shown as the green distribution in the background of Fig. 10. This beam is then tracked through the first carbon RFQ cavity field map without considering space charge effects. From the resulting beam at the end of the first cavity only the particles, which are accelerated to the nominal energy by the RFQ, are selected. The distribution corresponding to these accelerated particles at the RFQ entrance, the so-called Matching Plane (MP), characterizes the acceptance of the RFQ. The full 6D acceptance of the first carbon RFQ cavity is shown in Fig. 10 in comparison to the uniform beam used as input for the simulation. In both transverse phase spaces a similar normalized acceptance of about $0.21\,\mathrm{mm\,mrad}$ is estimated from the ellipse enclosing $95\,\%$ of the distribution at the RFQ MP corresponding to the accelerated particles. In addition, it is visible in the distribution of the acceptance beam in the longitudinal phase space that the acceptance of the RFQ is phase and energy dependent [14].

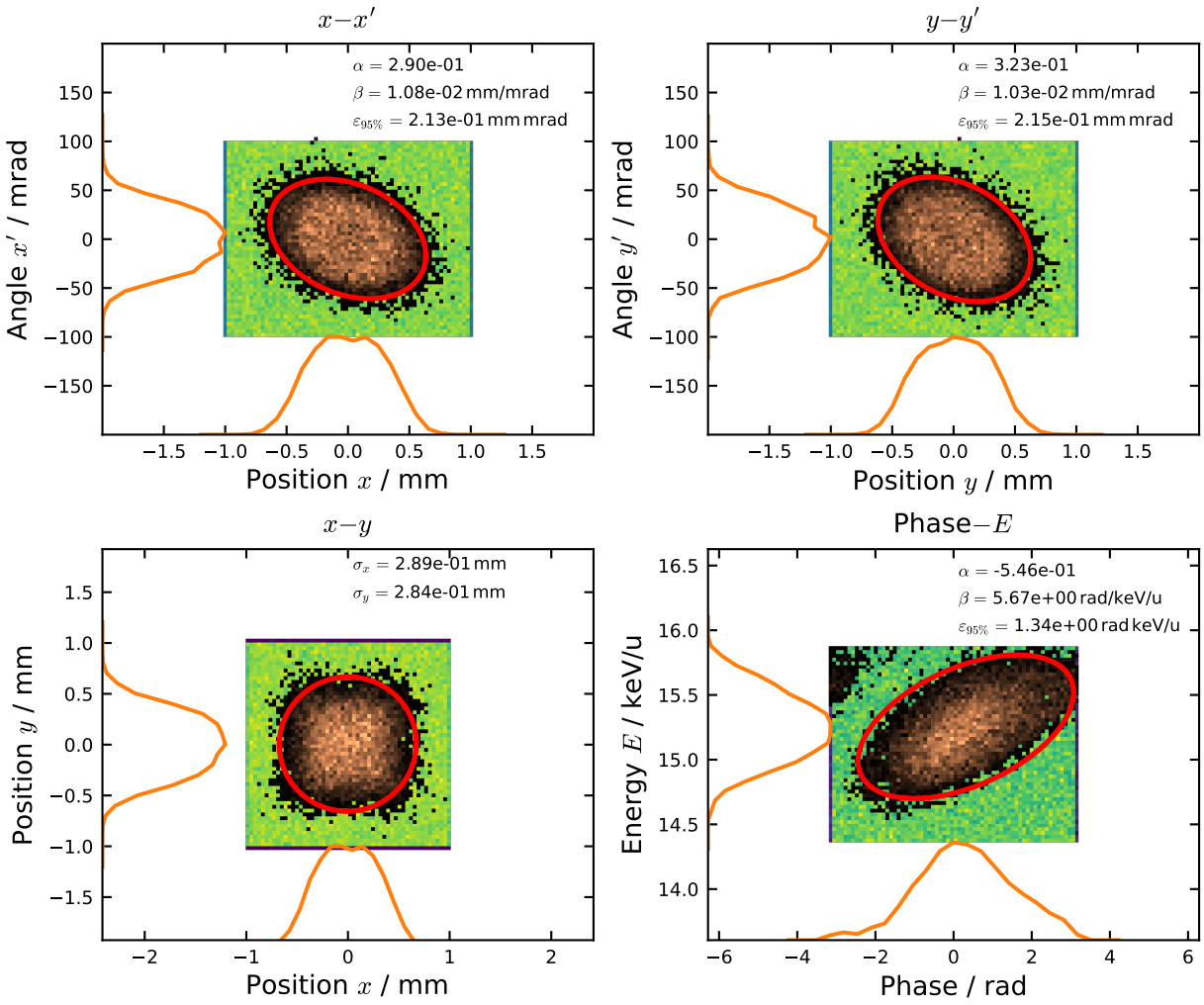

Figure 10: 6D phase space of the particle distribution accelerated by the first cavity of the carbon RFQ (copper-black distribution) remaining from a uniform fully stripped $^{12}C^{6+}$ carbon ion input beam (green distribution in the background) at the RFQ MP defining its acceptance. The full projections (orange) and the $95\,\%$ Twiss ellipses (red) are shown with the corresponding parameters.

The transverse phase space of the acceptance beam obtained by simulation has not such a clear edge as the example beam discussed in Section 2. Therefore, it will to some extent be necessary to cut outside particles with the acceptance box when defining the acceptance box aperture properties, so that the acceptance is not overestimated. To define the acceptance box parameters we will thus use a tracking simulation instead of direct calculation to determine the aperture positions from the phase advance and the aperture widths from the beam distribution at those positions. As discussed above, the transverse

acceptance of the RFQ depends on the energy and phase of the particles in the distribution. In this case we opted to average over all possibilities by using the 6D acceptance beam for the simulation.

The transverse phase advance is calculated from the transverse Twiss β-function, which is obtained by simulating a backward and forward drift of the acceptance beam from the RFQ MP. The aperture positions are determined as explained in Section 2.3, but from the simulation results as shown in Fig. 11. In addition, a $95\,\%$ beam size derived from the $95\,\%$ emittance and Twiss β-function via $\sigma = \sqrt{\varepsilon\beta}$ is shown together with the aperture positions. Small deviations are visible for the horizontal and vertical direction. However, the differences are not significant, thus the mean value is used for the four aperture positions for both dimensions.

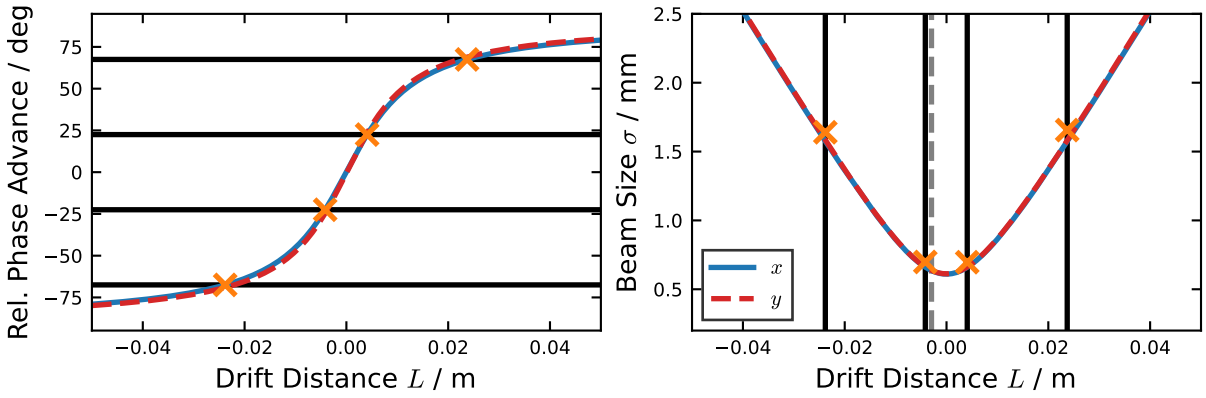

Figure 11: Determination of the acceptance box aperture positions for the carbon RFQ from the phase advance relative to the waist (left). The $95\,\%$ beam size derived from the $95\,\%$ emittance and Twiss β-function via $\sigma = \sqrt{\varepsilon\beta}$ is shown with the aperture positions and widths (right), but the aperture widths are defined by additionally analyzing the beam at the respective positions (see text). Note that the waist is still used a reference so that the minimum beam size is at $L = 0$ and $\psi(0) = 0$, while the reference beam at the RFQ MP is slightly behind the second aperture (dashed grey line).

The aperture widths are more difficult to define with an actual beam due to the outside sputtered particles. In this case we choose to aim for a transmission of about $95\,\%$ of the acceptance beam, i. e. loosing about $5\,\%$ of the outer beam parts in the acceptance box. Therefore, the aperture widths are increased somewhat in comparison to the $95\,\%$ beam size obtained above. In this case we set the aperture width to enclose $99\,\%$ of the particles in the respective dimension. This is illustrated in Fig. 12, where the shown beam distribution is drifted to the four aperture positions and the $99\,\%$ radii are indicated for both dimensions. Again, there are small but not significant differences in the two transverse dimensions, so the average can be used to have square apertures.

The exact parameters determined by simulation are however not crucial. It was confirmed in simulations that displacements of $\pm 5^\circ$ in phase advance or changes of the aperture below $0.1\,\mathrm{mm}$ do not significantly change the transmission through the acceptance box. Thus, the machining parameters are rounded up to $0.1\,\mathrm{mm}$. The final parameters of the carbon RFQ acceptance box apertures as it is constructed are summarized in Tab. 1 and are also indicated in Fig. 11 for comparison with the $95\,\%$ beam size. The apertures are squared and the full aperture is given.

Table 1: Carbon RFQ Acceptance Box Aperture Properties

Aperture	Width / mm	Distance to RFQ MP / mm	Distance Between / mm
1	3.4	−21.3	19.8
2	1.4	−1.5	7.6
3	1.4	6.1	19.0
4	3.4	25.1	

In reality the acceptance box consists of aperture plates and spacers, which are placed inside a dedicated vacuum tube. Thus, note that the aperture plates have a finite thickness, which In case of the

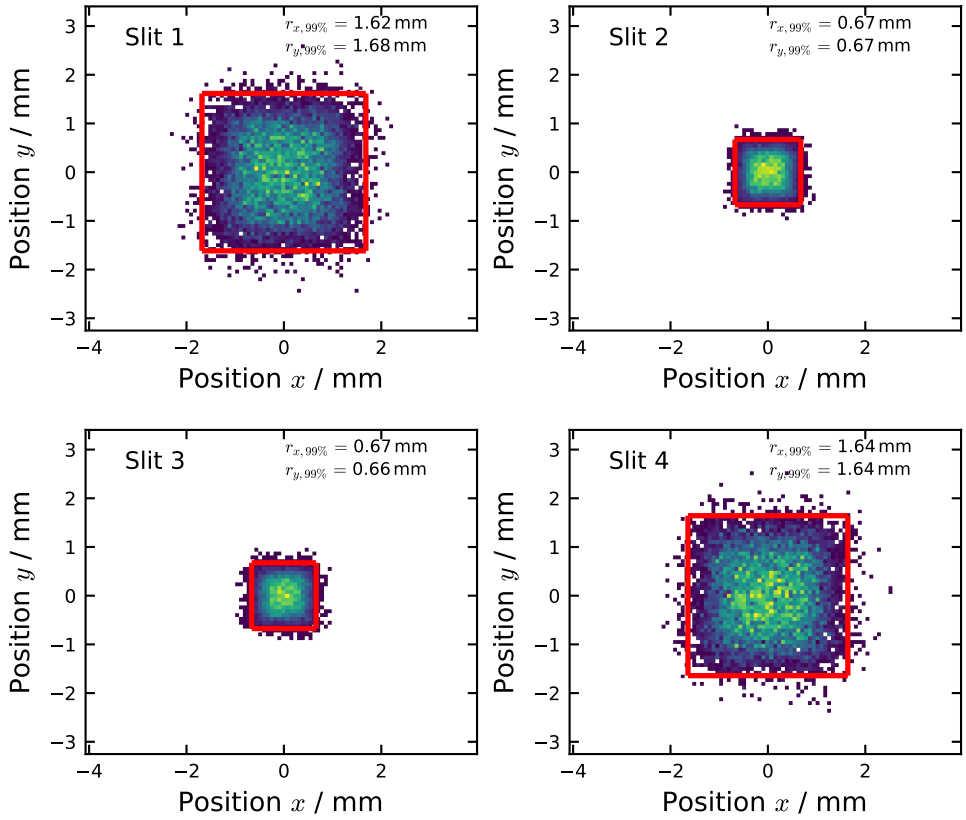

Figure 12: Beam distribution of carbon RFQ acceptance in the x-y-plane at the aperture positions determined in Fig. 11. The red ellipses indicate the region enclosing $95\,\%$ of the beam, the respective radii for the x and y dimension are given.

acceptance box of the carbon RFQ is $0.5\,\mathrm{mm}$. This thickness must then always be subtracted from the calculated drift distances between the apertures, to produce the respective spacers. The technical drawing of the carbon RFQ acceptance box and the first aperture are shown in Fig. 13.

The confined region of the acceptance box for the carbon RFQ is illustrated together with the transverse phase spaces of the RFQ acceptance at the RFQ MP in Fig. 14. The cuts according to the four apertures are indicated and the central beam region is transmitted. About $2.5\,\%$ of the particle distribution is outside of the cuts in each of the transverse dimensions. Thus considering independent distributions, in total about $5\,\%$ of the beam are not accepted.

3.2 ELISA / MACHINA RFQ Acceptance Box

Another very compact RFQ was developed at CERN based on the HF-RFQ design. Two copies of this RFQ are produced for different societal applications. One RFQ is used for the Movable Accelerator for Cultural Heritage In-situ Non-destructive Analysis (MACHINA) project, which transportable accelerator for the use in examining for example art with Proton Induced X-ray Emission (PIXE) [15]. The other RFQ is part of the Experimental LInac for Surface Analysis (ELISA) project as a accelerator demonstrator experiment installed at the CERN Science Gateway exhibition [16, 17].

The ELISA RFQ acceptance is again determined using a large uniform input beam in all dimensions and the RFQ acceptance defined by the particles accelerated to the nominal energy in the particle tracking simulation is shown together with the uniform input beam in Fig. 15. Space charge effects are again not considered, but do not play a role for this RFQ anyway, since only very low beam currents up to about $15\,\mathrm{mA}$ are the target for the ELISA source commissioning and only few µA are needed with MACHINA for PIXE studies, respectively.

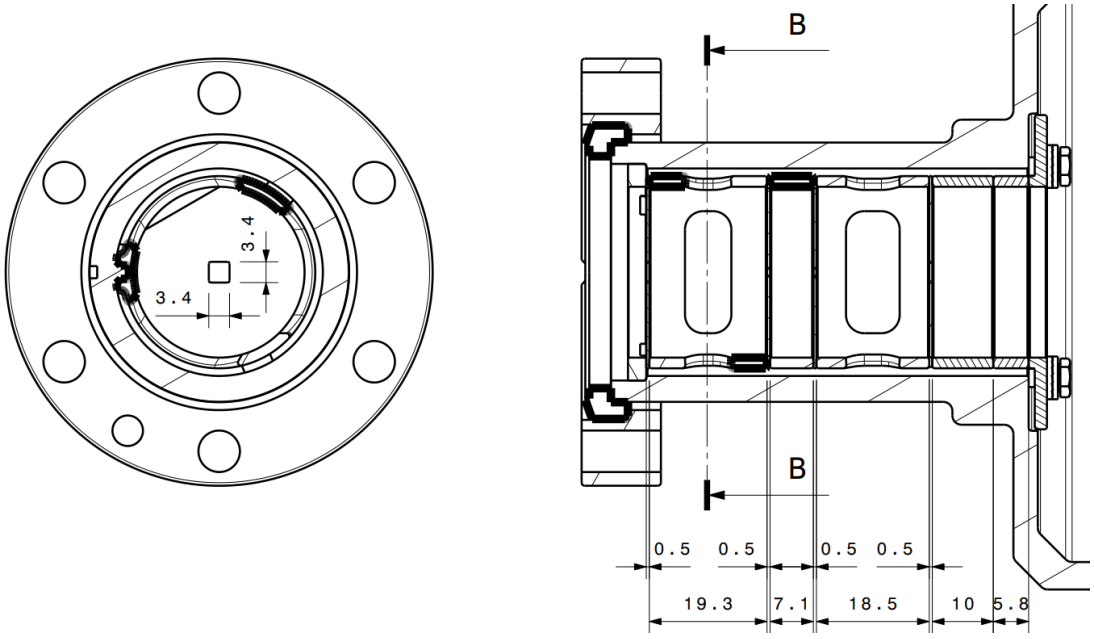

Figure 13: Technical drawing of carbon RFQ acceptance box: Front view with the first aperture blade (left) and side view (right, beam coming from the left), with indicated distances between the aperture plates and width of the first aperture.

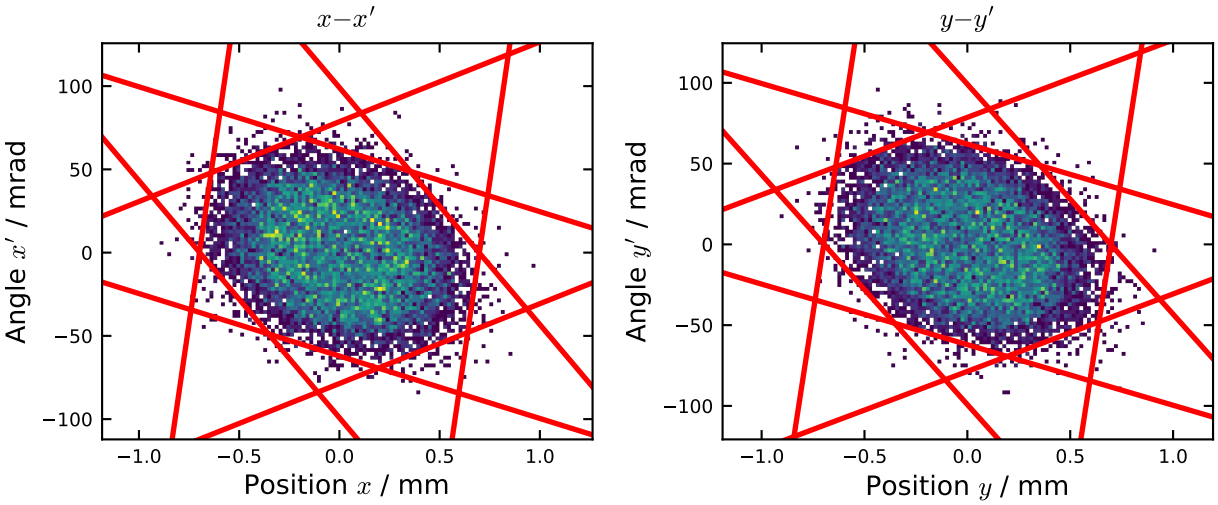

Figure 14: Illustration of region confined by the carbon RFQ acceptance box compared with the carbon RFQ acceptance in the x-x' and y-y'-phase spaces resulting in approximately $95\,\%$ transmission for the acceptance beam.

The ELISA RFQ acceptance is even more limited in the longitudinal phase space than the carbon RFQ, due to pushing for an even more compact design trading off longitudinal acceptance. The normalized transverse acceptance of about $0.33\,\mathrm{mm\,mrad}$ in both transverse dimensions is a bit larger than for the carbon RFQ.

The acceptance box parameters for ELISA/MACHINA RFQ are summarized in Tab. 2, again the squared and full apertures are given. The dimensions are a bit smaller than for the carbon RFQ acceptance box, although the transverse acceptance of the ELISA/MACHINA RFQ is bit larger. However, a more conservative acceptance box was designed due to the smaller longitudinal acceptance.

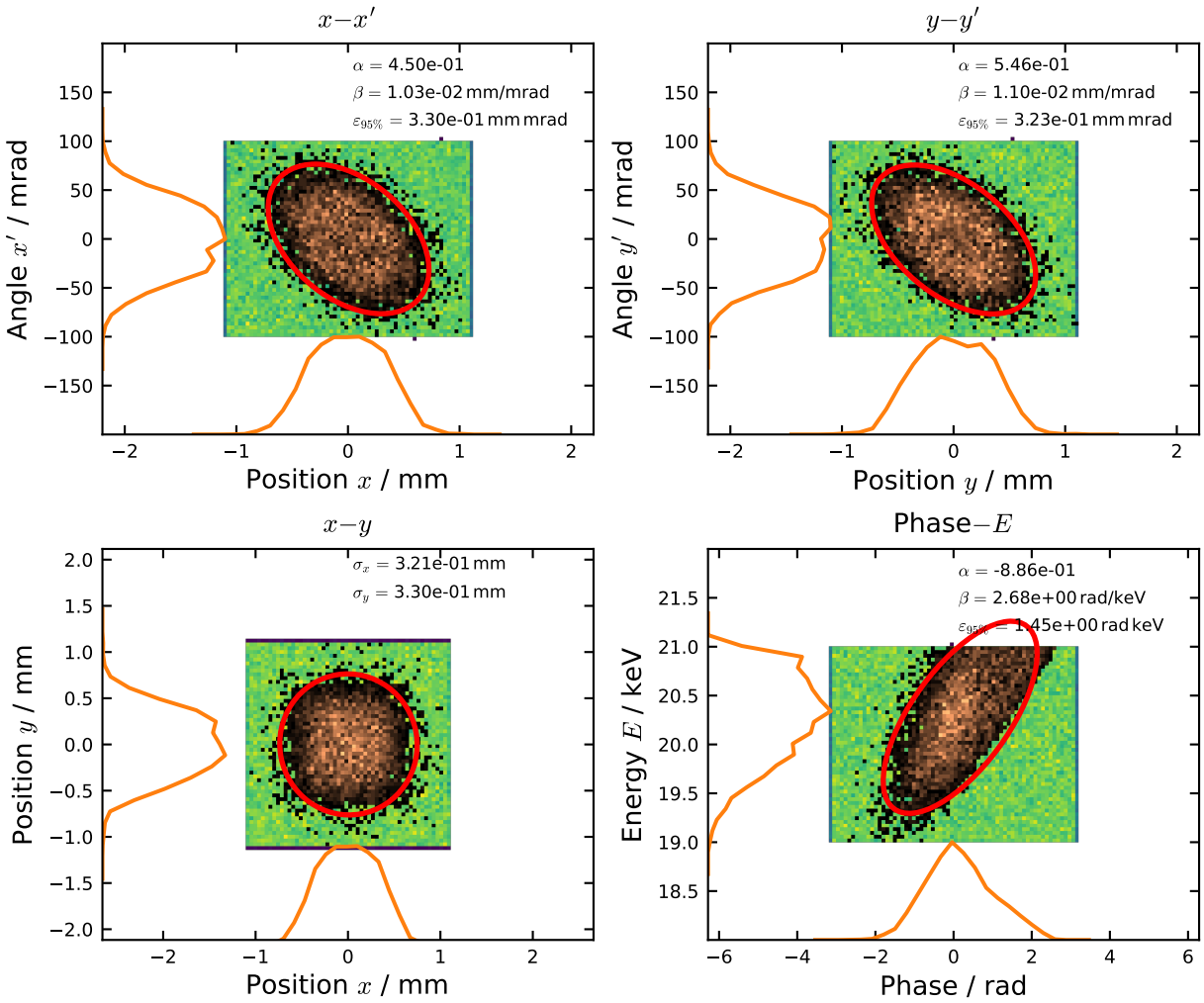

Figure 15: 6D phase space of the particle distribution corresponding to the particles accelerated by the ELISA/MACHINA RFQ (copper-black distribution) remaining from proton input beam (green distribution in the background) at the RFQ MP defining its acceptance. The full projections (orange) and the 95 % Twiss ellipses (red) are shown with the corresponding parameters.

Table 2: ELISA RFQ Acceptance Box Aperture Properties

Aperture	Width / mm	Distance to RFQ MP / mm	Distance Between / mm
1	2.8	−14.65	16.1
2	1.04	1.45	6.9
3	1.04	8.35	17.3
4	2.8	25.65	

3.3 Linac4 RFQ Acceptance Box

Linac4 is the injector for the CERN proton accelerator complex. It features a H^- source, a LEBT and an RFQ, before further acceleration with different Linac structures and finally injecting into the PS booster [18–20]. To do measurement test and preparations with spare sources as well as for developments of new sources an acceptance box is used at the source test stand at CERN to imitate the transverse acceptance of the Linac4 RFQ [3, 21–23]. The Linac4 RFQ operates at 352 MHz and accelerates the H^- ions from an input energy of 45 keV to 3 MeV [24].

The Linac4 RFQ acceptance is determined in the same way as for the carbon RFQ using a large uniform input beam in all dimensions. Although Linac4 provides much higher currents, still no space charge effects are considered to obtain the RFQ acceptance. The RFQ acceptance defined by the particles

accelerated to the nominal energy in the particle tracking simulation is shown together with the uniform input beam in Fig. 16.

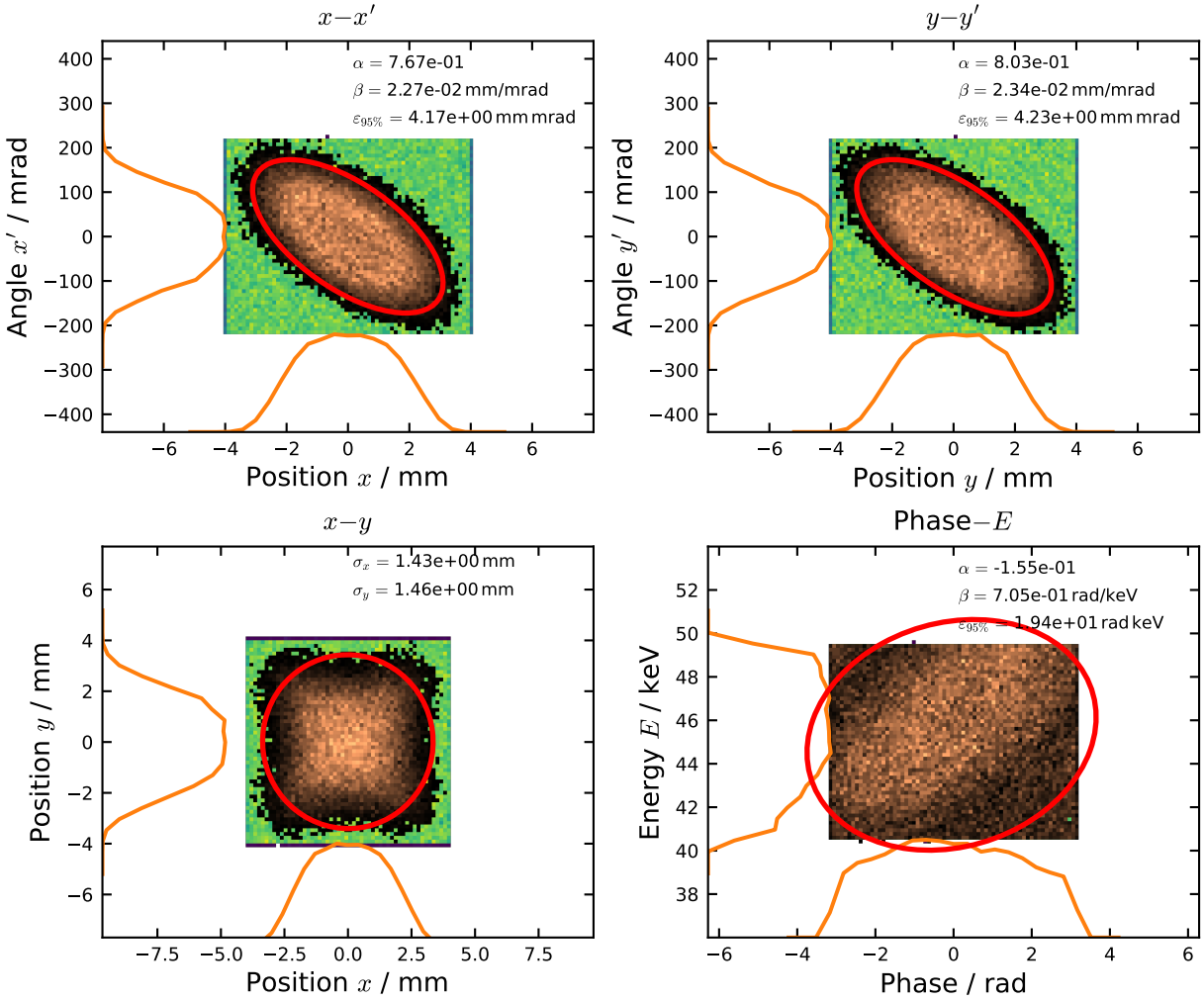

Figure 16: 6D phase space of the particle distribution corresponding to the particles accelerated by the Linac4 RFQ (copper-black distribution) remaining from H^- ion input beam (green distribution in the background) at the RFQ MP defining its acceptance. The full projections (orange) and the 95 % Twiss ellipses (red) are shown with the corresponding parameters.

It is apparent that the Linac4 RFQ has a much larger acceptance, since it is designed for a different purpose than the carbon RFQ. Operating at a lower frequency, the distance between RFQ vanes is larger and the RFQ thus accepts larger transverse dimensions. Furthermore, it is optimized for maximal transmission and is thus much less phase dependent than the carbon RFQ to capture and accelerate particles at all phases [5]. The majority of particles are accepted for all phases and energies even up to a relative energy spread of 10 %. Therefore, the Linac4 RFQ is mainly limited by the transverse acceptance, with a normalized acceptance of about 4.2 mm mrad in both transverse dimensions.

The parameters derived for the Linac4 RFQ acceptance box are summarized in Tab. 3, again the squared and full apertures are given. Due to the larger acceptance of the RFQ, the apertures are larger as for the carbon RFQ acceptance box. Furthermore, the distance between the apertures is longer since the Linac4 input beam energy is higher as for the carbon RFQ.

4 Validation and Measurements for Linac4

The performance of the acceptance box is validated in simulation and with measurements for the Linac4 RFQ, since experience has been gathered in multiple years of operation at Linac4 and for the source commissioning with the acceptance box. In addition, the Linac4 RFQ has the least losses in the longi-

Table 3: Linac4 RFQ Acceptance Box Aperture Properties

Aperture	Width / mm	Distance to RFQ MP / mm	Distance Between / mm
1	10.4	−20.0	26.7
2	4.34	6.7	11.4
3	4.34	18.1	24.2
4	9.8	42.3	

tudinal acceptance, so the transmission results are less different than for the ELISA and carbon RFQ. Two validation studies comparing the transmission through the Linac4 RFQ and the corresponding acceptance box are performed in Section 4.1. Finally, measurements at Linac4 and the source test stand are presented in Section 4.2.

4.1 Linac4 Acceptance Box Validation

As first test to verify that acceptance box represents the transverse RFQ acceptance the transmission of a variety of beams is compared for the RFQ and the acceptance box. The beams used for this study include beams with very different properties, e. g. regenerated from simulations or measurements, uniform, round, asymmetric, scaled and combination of these. The transverse phase-space at the RFQ MP of all beams used for this study can be found in the Appendix A.

The beams are tracked through the RFQ field map and through the acceptance box apertures in simulation without considering space charge effects. Note that for the simulation with the acceptance box, the beam is first tracked backward to the first aperture and then drifted forward, as the beam is generated at RFQ MP, which is downstream of the first aperture. The transmissions through the acceptance box and the Linac4 RFQ, where the latter considers only the particles which are accelerated, are compared in Fig. 17.

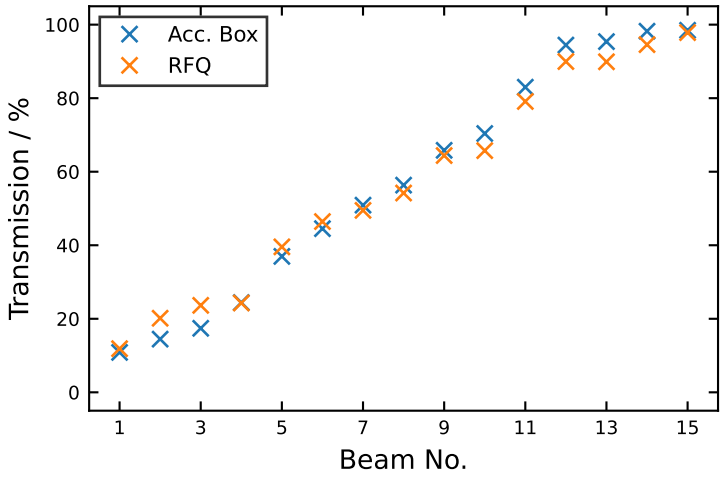

Figure 17: Comparison of the Linac4 acceptance box and RFQ transmission for different input beams sorted by increasing transmission through the acceptance box (see also Appendix A for the beams used for this study). For the RFQ transmission only particles accelerated to the nominal output energy are considered.

The acceptance box transmissions range from 10 % up to almost 100 %. The values for the transmissions through the RFQ and the general trend are clearly similar. Differences up to 5 % are obtained for a few beams, but for most beams only small deviations are observed. The transmissions for the RFQ are a bit better for low transmission beams as the acceptance box cuts a bit of the outer regions of the transverse acceptance. On the other hand, the acceptance box has a somewhat better transmission for beams with high transmissions, as it does not discriminate longitudinally. In reality the difference will increase due to space charge effects, which is considered in the following LEBT optimization study and is discussed for the measurements in Section 4.2.

A second simulation study to confirm the acceptance box performance is the optimization of the LEBT for the transmission through acceptance box and RFQ field map. An overview of the setup and devices of the LEBT at the Linac4 source test stand is shown together with the Linac RFQ acceptance box in Fig. 18. The optical elements are the same as for the LEBT installed at Linac4, transporting the beam from the source to the RFQ. It consists of two solenoids, two horizontal and vertical correctors, and additional diagnostic devices. The diagnostics includes the beam current transformer (BCT) for current measurements and slits plus SEM grids for emittance measurements.

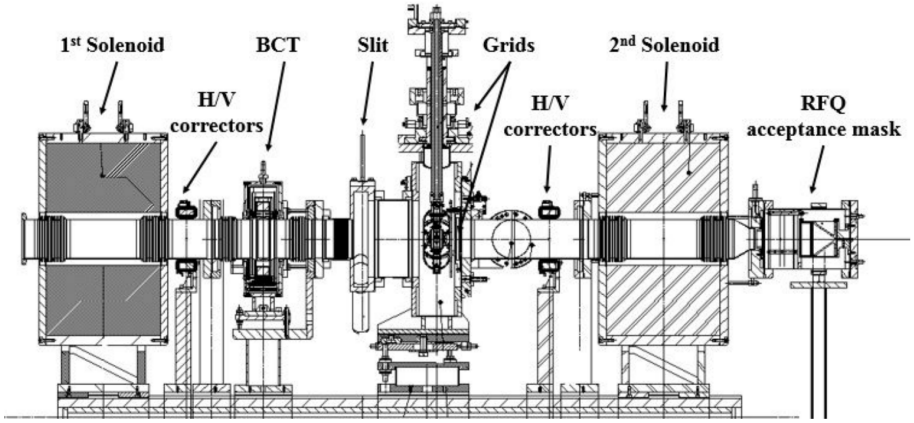

Figure 18: Linac4 test stand LEBT layout with the RFQ acceptance box [3].

As starting point for the optimization the beam shown in Fig. 19 is used. The horizontal and vertical beam emittance was measured with the slit and the SEM grid in the LEBT and the corresponding beam distribution has been created for the simulation. The beam at the measurement position is then tracked backwards in simulation to the start of the LEBT to the output plane of the source considering the setting of the first solenoid.

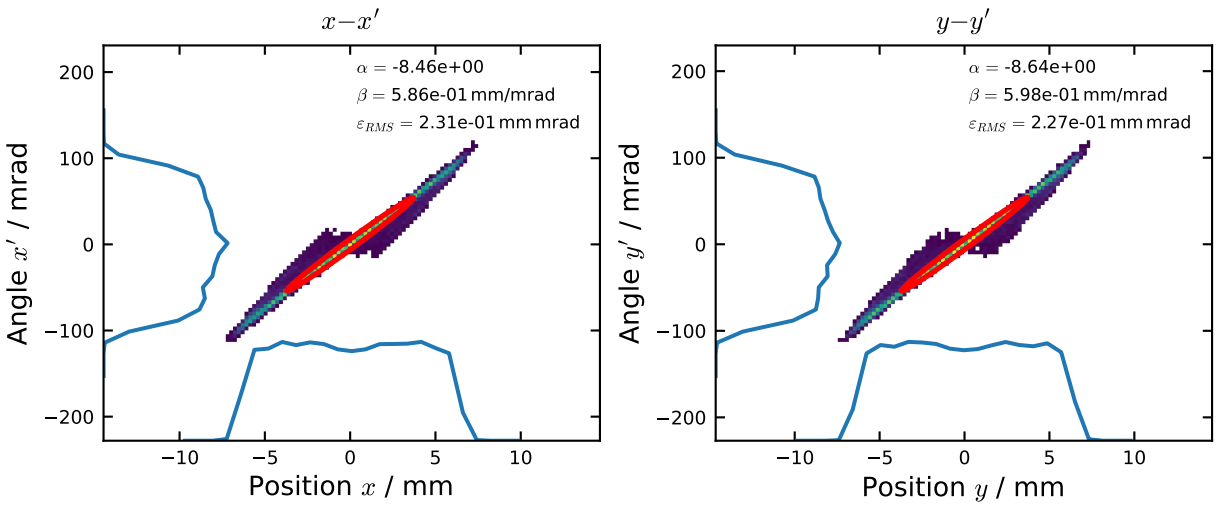

Figure 19: Transverse phase spaces of the Linac4 source test stand LEBT input beam. Created based on emittance measurements in the LEBT (Fig. 18) and tracked backwards to the source output plane.

Apart from the steerers for correcting the beam position and angle, the two knobs to focus and match the beam at the RFQ MP are the solenoids in the LEBT. Both solenoid currents were changed in the range of $80\,\mathrm{mA}$ to $125\,\mathrm{mA}$ and the complete setup is simulated separately with the acceptance box and the RFQ. The simulations are run with space charge effects at a beam current of $35\,\mathrm{mA}$, but in the LEBT $90\,\%$ space charge compensations is considered, thus the beam current in the LEBT is set to $3.5\,\mathrm{mA}$. The transmission through the acceptance box and the RFQ field map in simulation are shown as function of the solenoid currents in Fig. 20. Note that the simulation scan with the RFQ is performed with coarser steps due to this simulation being much more time intensive.

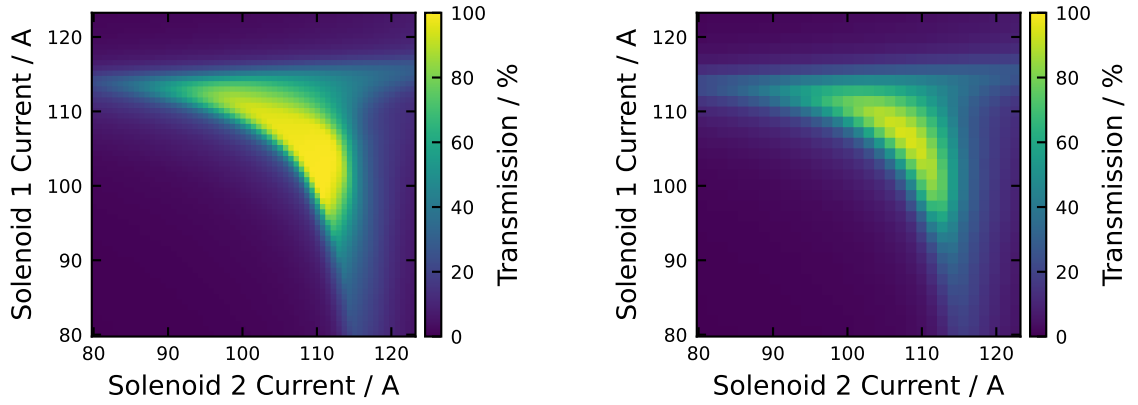

Figure 20: Comparison of the simulated transmission through the acceptance box (left) and the RFQ field map (right) of the beam out of the source shown in Fig. 19 as function of the solenoid current settings in the LEBT considering a beam current of $35\,\mathrm{mA}$ and $90\,\%$ space charge compensation in the LEBT.

The regions of high transmission have a similar bow-like shape with a maximum around both solenoids set to about $110\,\mathrm{mA}$ for the acceptance box and the RFQ. However, as expected the transmission through the acceptance box is in general a bit higher and the region of transmissions above $90\,\%$ is larger. The optimal transmission of $94.1\,\%$ through the RFQ was achieved with the solenoids set to $105.85\,\mathrm{A}$ and $108.75\,\mathrm{A}$, respectively. The transverse phase space of the corresponding beam was also used as beam 15 for the transmission comparison test and is shown in Fig. A.15 in Appendix A. For these settings the transmission through the acceptance box is $98.5\,\%$. This is however not the highest value for the acceptance box and transmission up to $99\,\%$ can be achieved for several combinations.

4.2 Linac4 and Source Test Stand Measurements

Measurements of the transmission through the Linac4 RFQ and the corresponding acceptance box have been performed for two different sources (IS03 and IS04) at Linac4 and at the Linac4 source test stand, respectively [21, 22]. The transmitted beam current is measured as a function of the input beam current from the source ranging from $20\,\mathrm{mA}$ up to $60\,\mathrm{mA}$. The solenoid settings are optimized for each single measurement configuration. The absolute transmitted beam current and the relative transmission of RFQ transmission and acceptance box are compared in Fig. 21 for both sources. The input beam currents were in both cases measured with the BCT in the LEBT (see Fig. 18. The transmitted beam current was measured with a BCT downstream the RFQ and with a Faraday cup behind the acceptance box [22, 23].

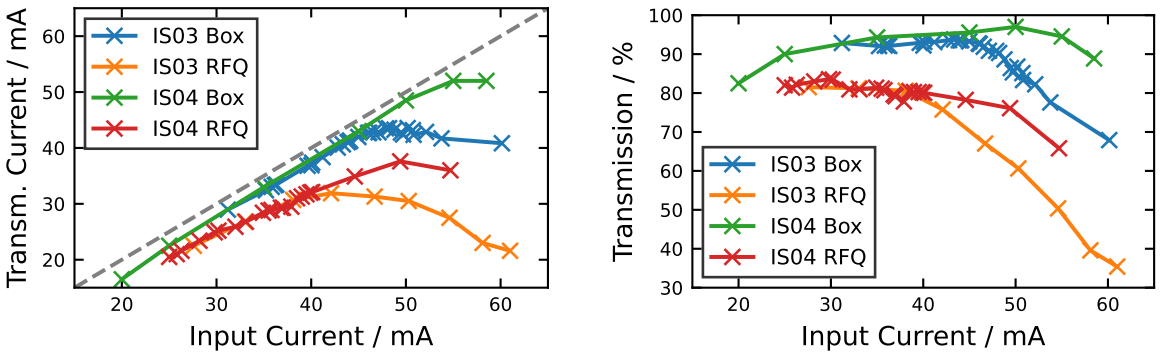

Figure 21: Measurements of total transmitted current (left) and relative transmission (right) for the IS03 and IS04 sources at Linac4 through the RFQ and the Linac4 test stand through the acceptance box, respectively [22, 23].

While as expected the transmission through the acceptance box is higher in all cases, the trend for the transmission through the RFQ and the acceptance box are similar. With the acceptance box transmissions over $90\,\%$ can be achieved for a wide range of source currents. For the RFQ the transmission is also quite

stable, but around $80\,\%$, for currents up to $40\,\mathrm{mA}$. The difference between the two different source types is small for both, RFQ and acceptance box, below $40\,\mathrm{mA}$. For higher currents the transmission is better for the IS04, which has a better beam quality for higher currents.

Admittedly, the transmission measurements can never be made under the exact same circumstances with the RFQ and the acceptance box and were in this case made in different setups. Even when using the same source and LEBT setup, there are always differences between the setups apart from minor drifts or changes, since the measurements with the RFQ and the acceptance box cannot be done at the same time. The same would however be the case for any other diagnostics. As explained above for the simulation results shown in Fig. 17, the acceptance box does not discriminate any longitudinal losses, or any other correlation in general. In addition, space charge effects are reducing the transmission through the RFQ even more for higher currents. Thus, it is in any case advised to perform complementary beam dynamics simulations to understand and verify the results.

Further measurements are foreseen at the Linac4 source test stand, especially for the commissioning and validation of the Linac4 spare RFQ. A solenoid scan is planned to have the transmission comparison shown in Fig. 20 also for measurements.

5 Conclusion

The concept of the acceptance box enclosing a transverse phase space has been introduced and derived based on the transverse phase advance. Further, a recipe for the definition the acceptance box parameters for a transverse beam distribution has been given. At CERN three acceptance boxes for RFQs have been designed and are used successfully for source and LEBT commissioning and optimization. The performance of the Linac4 RFQ acceptance box has been validated by simulations and measurements of the transmission through the RFQ and the acceptance box. More results will be available as the commissioning of the ELISA RFQ is ongoing and the carbon RFQ will be delivered soon.

In conclusion, the acceptance box is an essential ingredient for a source test stand and proved to be a valuable tool. It is an efficient, robust and simple device for fast source and LEBT optimization. It is much cheaper in comparison to typical emittance measurement methods, and does not require a specific analysis. Currently, acceptance boxes are used in Linacs at low energies in the range of some ten keVs. Especially imitating the transverse acceptance of an RFQ, they represent a cheap and efficient method to prepare sources without needing the RFQ itself. However, the use case of acceptance boxes can be extended within reasonable distances up to energies of a few MeV, whenever a quick method is needed to obtain the ratio of beam inside a certain transverse emittance.

6 Acknowledgements

The authors thank the HSL section for many discussions on the acceptance box and acceptance of RFQs. The authors thank Angel Rodriguez (CIEMAT) for providing the drawings of the carbon RFQ acceptance box shown in Fig. 13.

7 References

[1] E. Bravin, “Transverse emittance”, *Proceedings of the course on Beam Instrumentation for Particle Accelerators* (CERN Accelerator School, Tuusula, Finland, Jun. 2018), pp. 442–455, URL: http://cds.cern.ch/record/2625174.

[2] G. Bellodi et al., “LINAC4 45 keV Proton Beam Measurements”, *Proc. LINAC’12* (Tel-Aviv, Isreal, Sep. 2012), pp. 867–869, URL: https://accelconf.web.cern.ch/linac2012/papers/thpb011.pdf.

[3] J.-B. Lallement et al., “Activities at the Linac4 Test Stand”, *Proc. LINAC’18* (Beijing, China, Sep. 2018), pp. 587–590, DOI: 10.18429/JACoW-LINAC2018-TUPO127.

[4] H. Wiedemann, *Particle Accelerator Physics*, 3rd ed., Berlin, Heidelberg: Springer, 2007.

[5] G. R. Montoya-Soto et al., “Study of longitudinal mechanisms and correlations in the definition of RFQ transverse acceptance”, *AIP Advances* 13.5 (2023), p. 055105, DOI: 10.1063/5.0145935.

[6] A. M. Lombardi et al., "High Frequency Compact Low-Energy Linear Accelerator Design", European Patent No. EP 3 180 966 B1, European Patent Office, 2014.

[7] M. Vretenar et al., "A Compact High-Frequency RFQ for Medical Applications", *Proc. LINAC'14* (Geneva, Switzerland, Aug.-Sep. 2014, paper THPP040), pp. 935–938, URL: http://cds.cern.ch/record/2062619.

[8] A. Degiovanni, P. Stabile, and D. Ungaro, "LIGHT: A Linear Accelerator for Proton Therapy", *Proc. NAPAC'16* (Chicago, IL, USA, Oct. 2016), pp. 1282–1286, DOI: 10.18429/JACoW-NAPAC2016-FRB1IO02.

[9] H. Pommerenke, "Compact radio-frequency quadrupoles for industrial and medical applications", PhD thesis, Universität Rostok, Germany, 2020, DOI: 10.18453/rosdok_id00002956.

[10] V. Bencini et al., "750 MHz radio frequency quadrupole with trapezoidal vanes for carbon ion therapy", *Phys. Rev. Accel. Beams* 23 (2020), p. 122003, DOI: 10.1103/PhysRevAccelBeams.23.122003.

[11] V. Bencini, "Design of a novel linear accelerator for carbon ion therapy", PhD thesis, La Sapienza, Universita di Roma, Italy, 2019, URL: https://cds.cern.ch/record/2711219.

[12] CERN, *Travel*, version 4.06, 2019.

[13] COMSOL Multiphysics GmbH, *COMSOL Multiphysics®*, URL: https://www.comsol.com.

[14] M. Koopmans et al., "Preparations for beam commissioning of the carbon RFQ at CERN", *Proc. IPAC'23* (Venice, Italy, May 2023), pp. 5020–5023, DOI: 10.18429/JACoW-IPAC2023-THPM057.

[15] S. Mathot et al., "The CERN PIXE-RFQ, a transportable proton accelerator for the MACHINA project", *Nuclear Instruments and Methods in Physics Research Section B: Beam Interactions with Materials and Atoms* 459 (2019), pp. 153–157, DOI: https://doi.org/10.1016/j.nimb.2019.08.025.

[16] S. Mathot et al., "ELISA Technical Design Report", CERN, Geneva, Switzerland, to be published.

[17] E. Pasino et al., "ELISA: a compact linear accelerator for societal applications", *Proc. IPAC'24* (Nashville, TN, USA, May 2024), pp. 3471–3474, DOI: 10.18429/JACoW-IPAC2024-THPR01.

[18] L. Arnaudon et al., "Linac4 Technical Design Report", CERN, Geneva, Switzerland, Rep. CERN-AB-2006-084, 2006, URL: https://cds.cern.ch/record/1004186.

[19] M. Vretenar et al., "The Linac4 Project at CERN", *Proc. IPAC'11* (San Sebastian, Spain, Sep. 2011), pp. 900–902, URL: https://accelconf.web.cern.ch/ipac2011/papers/tuoaa03.pdf.

[20] A. Lombardi, "Commissioning of CERN LINAC4", *Proc. LINAC'18* (Beijing, China, Sep. 2018), pp. 658–662, DOI: 10.18429/JACoW-LINAC2018-TH1P01.

[21] J. Etxebarria et al., "Characterization of IS04 H^- ion source for CERN's LINAC4", CERN, Geneva, Switzerland, Rep. CERN-ACC-NOTE-2023-0016 (internal), 2023.

[22] E. Sargsyan et al., "Linac4 Source and Low Energy Experience and Challenges", *Proc. HB'23* (Geneva, Switzerland, Oct. 2023), pp. 290–296, DOI: 10.18429/JACoW-HB2023-WEA4I2.

[23] E. Sargsyan et al., "Operational experience and reliability of the new CERN Linac4", *Proc. Linac'24* (Chicago, IL, USA, Aug. 2024), pp. 636–641, DOI: 10.18429/JACoW-LINAC2024-FRXA004.

[24] C. Rossi et al., "Commissioning and Operational Experience Gained with the Linac4 RFQ at CERN", *Proc. LINAC'14* (Geneva, Switzerland, Aug.-Sep. 2014), pp. 926–928, URL: https://cds.cern.ch/record/2062616.

Appendix

A Beams for Acceptance Box Validation

This appendix section complements the acceptance box validation studies in Section 4.1. The transmission of the beams through the acceptance box and the RFQ field map without space charge effects corresponding to the results shown in Fig. 17 are summarized in Tab. A.1 using the same numbering increasing with transmission through the acceptance box. The transverse phase spaces of the beams used for the study are shown in the following in Figs. A.1 to A.15. Different distributions have been used or created, e. g. uniform or binomial distributed beams with different shapes (Figs. A.1 to A.4), matched or mismatched beams with different emittances (Figs. A.5 to A.11 and A.14), beams created based on measurements (Figs. A.11 and A.12, [21]), and the optimized beam from the solenoid scan study in Section 4.1 (Fig. A.15). The transverse acceptance ellipse of the Linac4 RFQ is shown as red dashed ellipse in all phase-space plots as reference. The energy is set to $45\,\mathrm{keV}$ with $1\,\%$ RMS relative energy spread and the longitudinal phase is uniform for all beams.

Table A.1: Transmissions through the Linac4 RFQ Acceptance Box and the Linac4 RFQ shown in Fig. 17

Beam No.	Phase-Space Plot	Acc. Box Transmission / %	RFQ Transmission / %
1	Fig. A.1	10.9	11.9
2	Fig. A.2	14.5	20.1
3	Fig. A.3	17.4	23.7
4	Fig. A.4	24.4	24.3
5	Fig. A.5	37.0	39.6
6	Fig. A.6	44.5	46.4
7	Fig. A.7	50.9	49.5
8	Fig. A.8	56.3	54.2
9	Fig. A.9	65.8	64.4
10	Fig. A.10	70.4	65.7
11	Fig. A.11	83.0	79.1
12	Fig. A.12	94.4	90.0
13	Fig. A.13	95.4	89.9
14	Fig. A.14	98.2	94.6
15	Fig. A.15	98.5	97.8

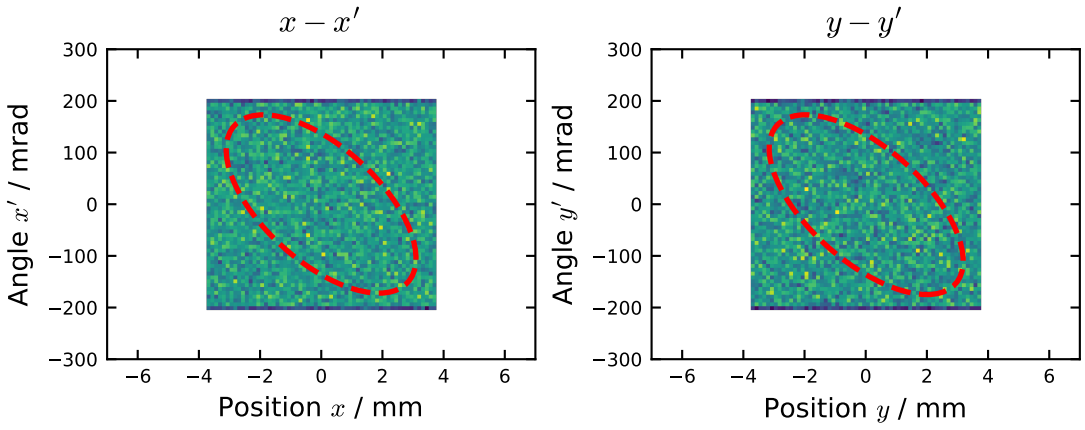

Figure A.1: Transverse phase space distribution of beam 1.

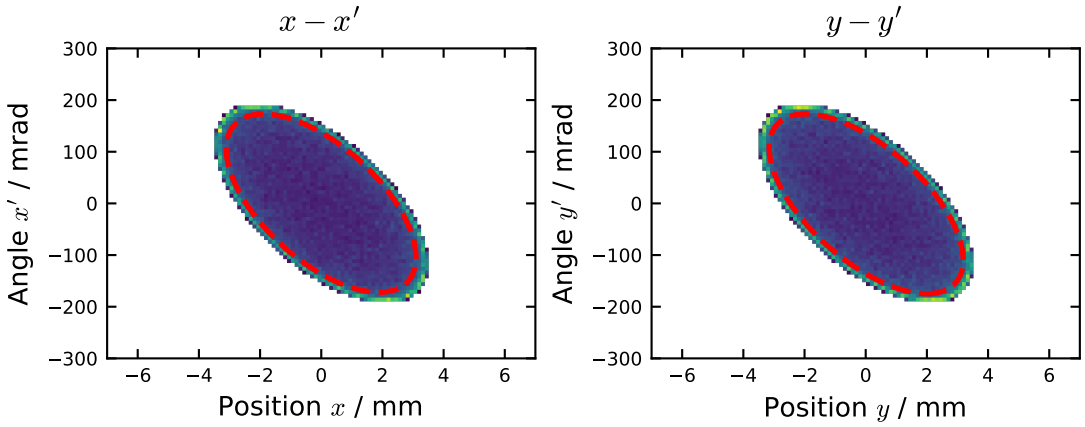

Figure A.2: Transverse phase space distribution of beam 2.

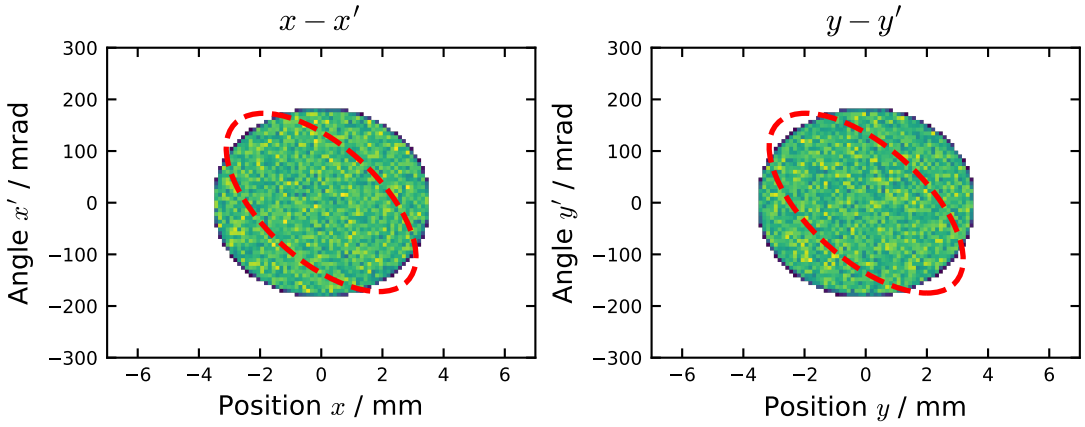

Figure A.3: Transverse phase space distribution of beam 3.

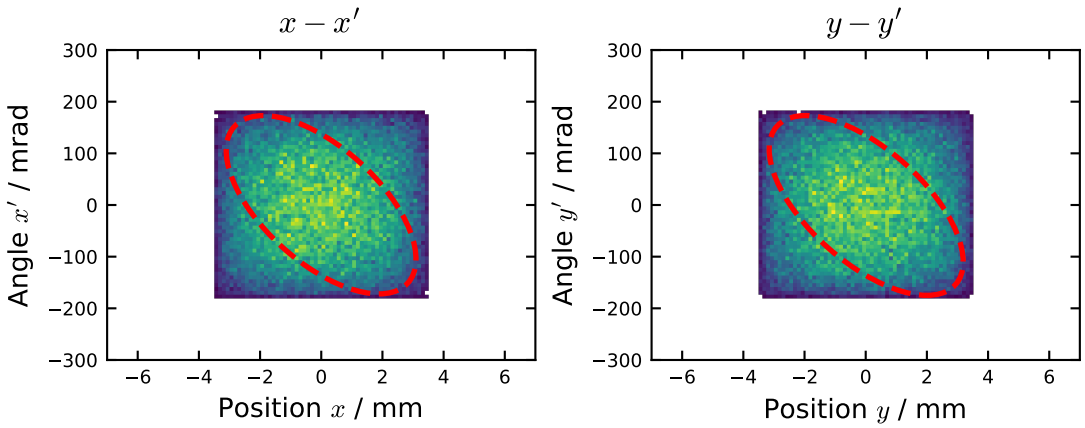

Figure A.4: Transverse phase space distribution of beam 4.

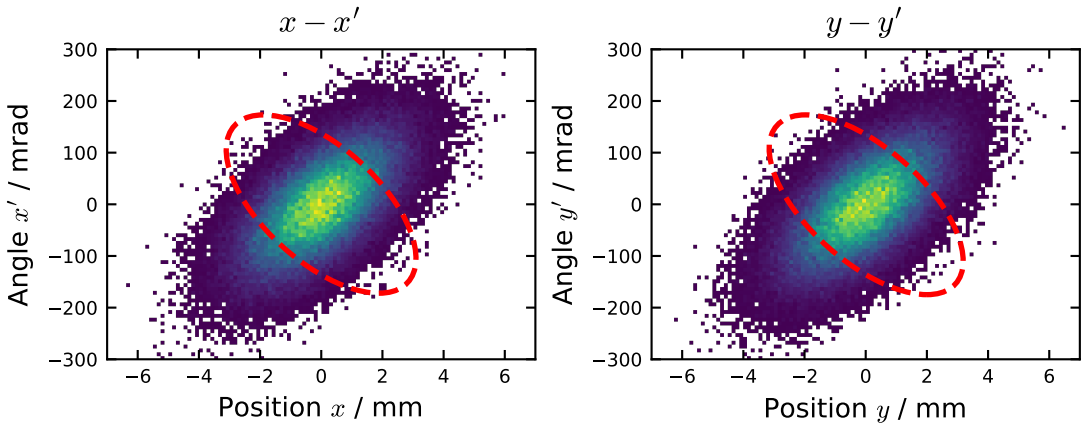

Figure A.5: Transverse phase space distribution of beam 5.

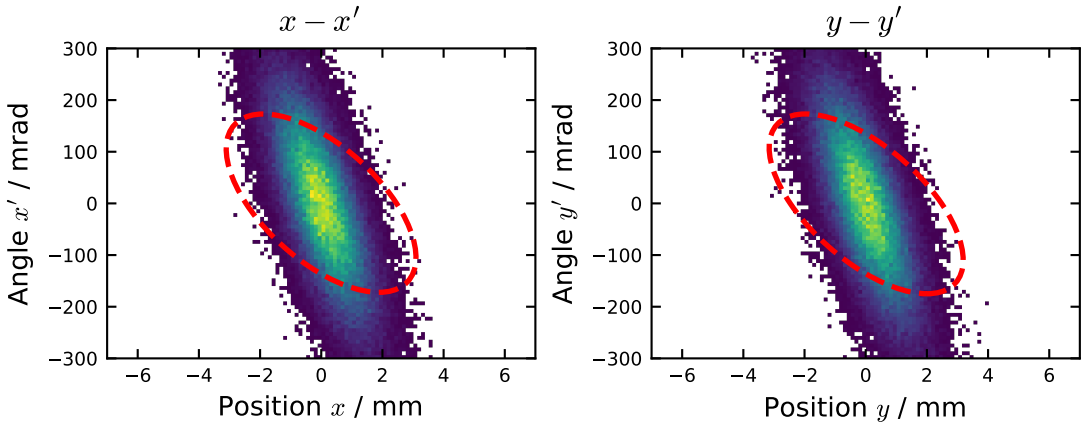

Figure A.6: Transverse phase space distribution of beam 6.

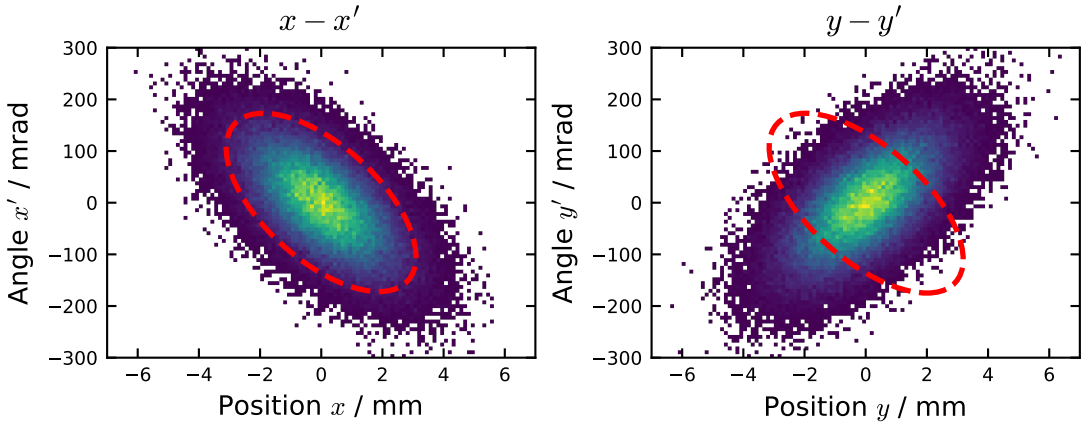

Figure A.7: Transverse phase space distribution of beam 7.

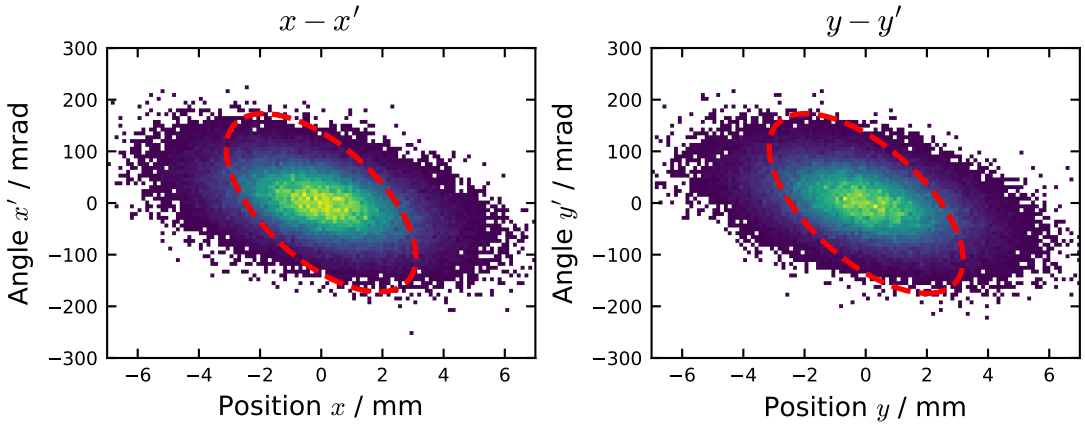

Figure A.8: Transverse phase space distribution of beam 8.

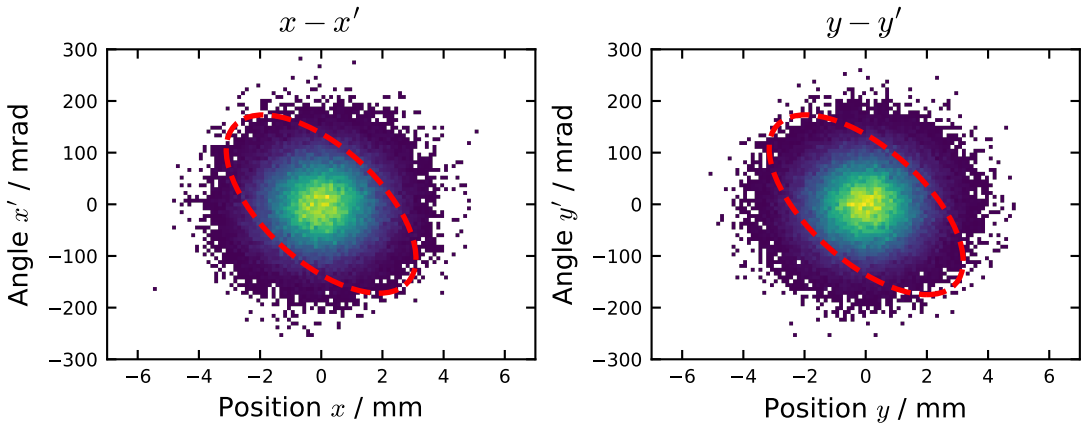

Figure A.9: Transverse phase space distribution of beam 9.

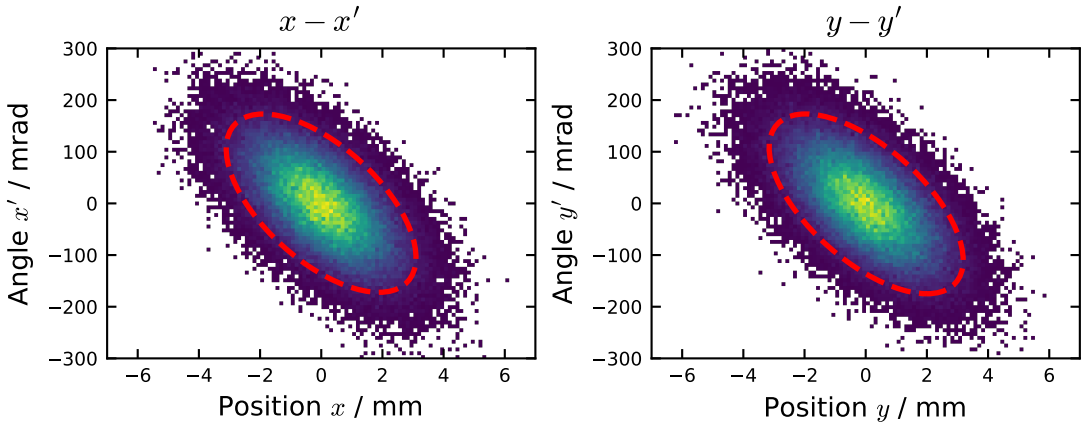

Figure A.10: Transverse phase space distribution of beam 10.

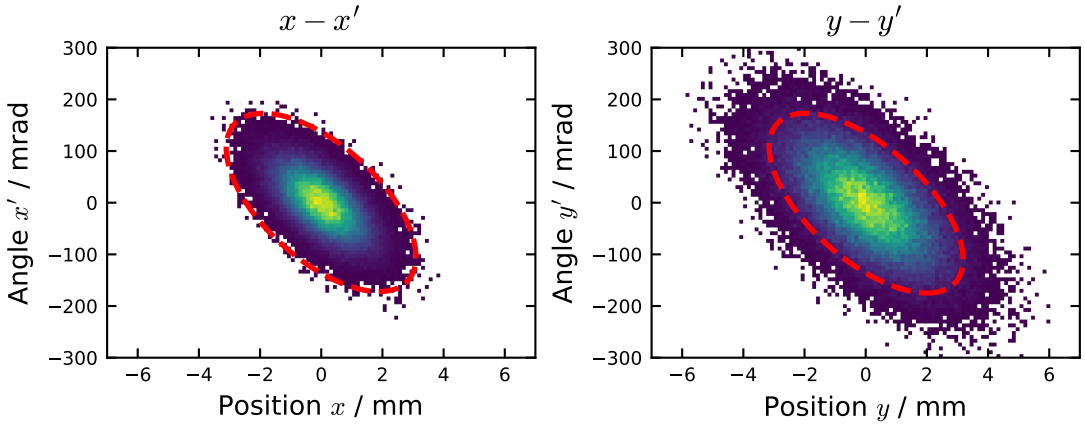

Figure A.11: Transverse phase space distribution of beam 11.

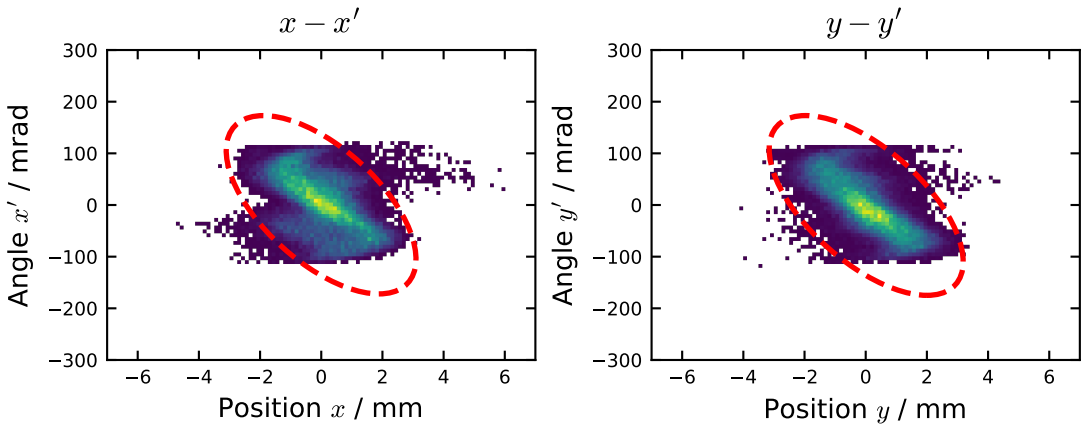

Figure A.12: Transverse phase space distribution of beam 12.

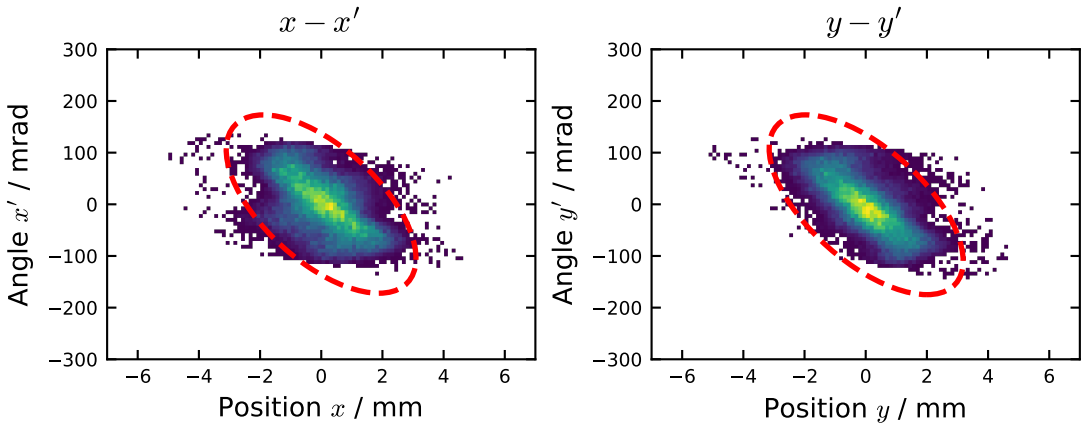

Figure A.13: Transverse phase space distribution of beam 13.

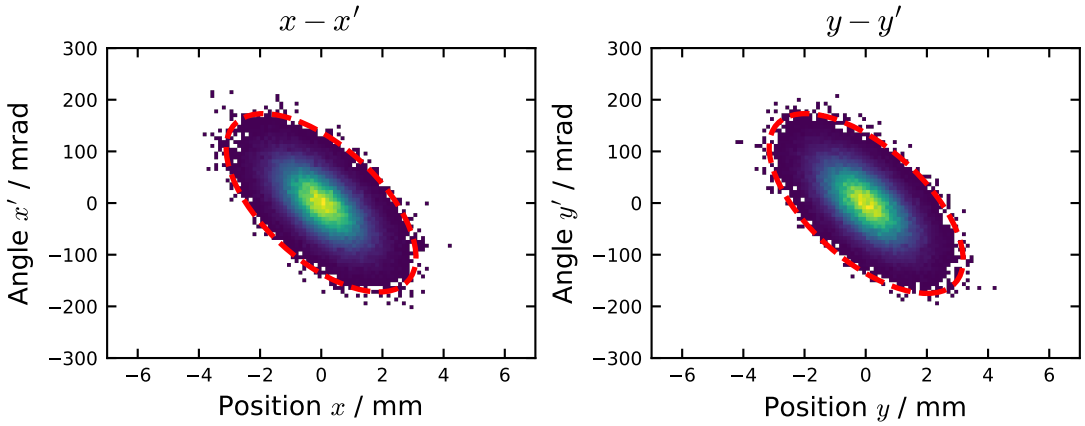

Figure A.14: Transverse phase space distribution of beam 14.

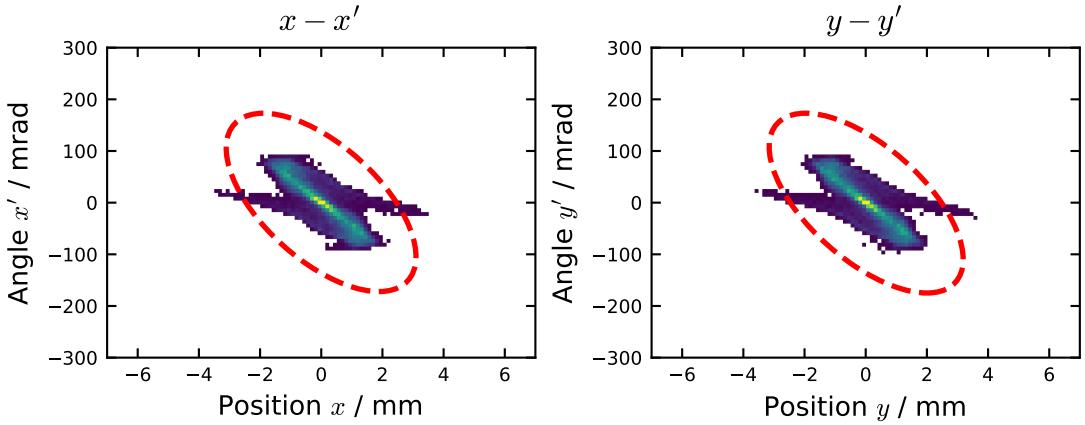

Figure A.15: Transverse phase space distribution of beam 15.

B Used Acceptance Box Plates

Fig. B.1 shows some images of apertures used for the first aperture of the Linac4 RFQ acceptance box at the Linac4 source test stand. The apertures in the top images have been used with mostly focused beams and it is visible that the metal starts to melt at the surface. The aperture in the lower left has been exposed to a less focused beam and a larger beam spot is visible. The aperture in the lower right was used during a steerer scan, resulting in a regular pattern.

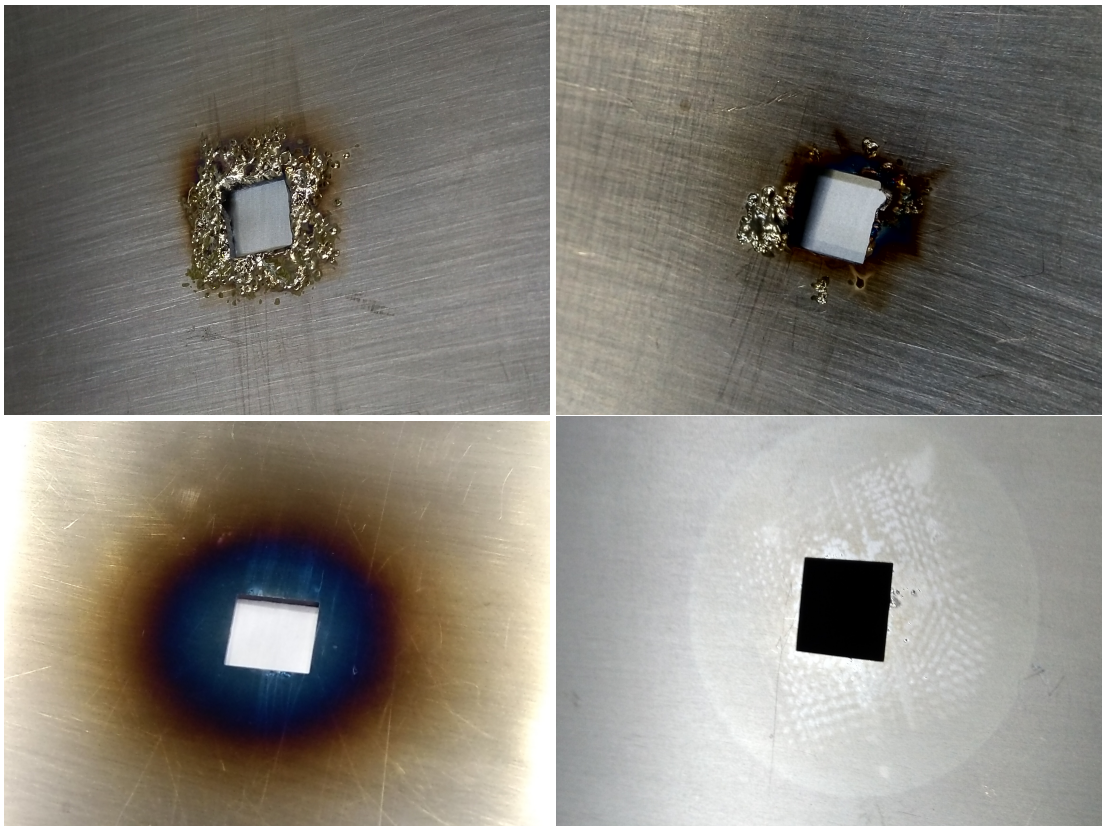

Figure B.1: Images of apertures used for the first aperture of the Linac4 RFQ acceptance box at the Linac4 source test stand.